

# The Bafoussam volcanic series: origin and evolution of the volcanism along the Cameroon volcanic line

Philippe Essomba<sup>1</sup> · Gilles Chazot<sup>2</sup>  · Nicaise Blaise Tchuimegnie Ngongang<sup>3</sup> · Arnaud Agranier<sup>2</sup> · Pierre Kamgang<sup>1</sup> · Hervé Bellon<sup>2</sup> · Philippe Nonnotte<sup>2</sup> · Pierre Wotchoko<sup>4</sup> · Innocent Badriyo<sup>1,5</sup>

Received: 29 April 2022 / Revised: 7 July 2022 / Accepted: 14 July 2022 / Published online: 11 August 2022

© The Author(s), under exclusive licence to Science Press and Institute of Geochemistry, CAS and Springer-Verlag GmbH Germany, part of Springer Nature 2022

**Abstract** The Bafoussam area in western Cameroon is part of the central Cameroon Volcanic Line (CVL). This study presents the mineralogy, major and trace element compositions, Sr-Pb-Hf isotopes, and new K-Ar geochronological data about mafic and felsic volcanic rocks. These rocks belong to two different series: A transitional series made of basalts, basaltic andesite, and trachytes and an alkaline mafic series with basalts, hawaiites, and basanites. New age data show that the transitional series belongs to the oldest part of the CVL and was emplaced between 47 and 35 Ma. The alkaline volcanism is younger, with ages ranging from 10 to 4.5 Ma.

Magmatic evolution in both series is accomplished through a fractional crystallization process, with the removal of olivine and clinopyroxene, while plagioclase does not seem to be a major crystallizing phase. All the samples are enriched in incompatible trace elements, but the rocks from the alkaline series have more fractionated REE patterns and high Nb content compared to the

transitional mafic lavas. Alkaline lavas have lower initial  $^{87}\text{Sr}/^{86}\text{Sr}$  and higher  $^{176}\text{Hf}/^{177}\text{Hf}$  and Pb isotopic ratios than the transitional lavas.

Low La/Nb and high  $^{87}\text{Sr}/^{86}\text{Sr}$  ratio are among chemical characteristics that show that some samples from the transitional series have interacted with a crustal component during their evolution in the crust. They cannot be used for discussing the mantle source of the volcanic rocks from this series. Trace elements show that primary magmas for both series formed in a garnet-bearing mantle source, with higher partial melting degrees (3–5%) for the transitional magmas than for the alkaline magmas (< 2.5%). Combining trace elements and isotopic ratios, we show that the Bafoussam lavas formed from two different mantle sources. Transitional magmas formed from a pyroxenite-bearing enriched mantle with low Pb isotopic composition. This mantle source is present in all the oldest lavas from the CVL. Alkaline magmas formed from an HIMU-like mantle source, different from the Mt Cameroon HIMU mantle source. The depleted asthenospheric mantle is not involved in the Bafoussam magmatism and the two mantle sources are probably located in the lithospheric mantle, in agreement with recent geophysical models presenting the CVL as a consequence of the partial melting of the lithospheric mantle in response to edge convection along the margin of the Congo craton.

**Keywords** Cameroon Volcanic Line · Bafoussam · Mafic volcanic rocks · Felsic volcanic rocks · Mantle source

✉ Gilles Chazot  
Gilles.Chazot@univ-brest.fr

<sup>1</sup> Département Des Sciences de La Terre, Faculté Des Sciences, Université de Yaoundé I, B.P. 812 Yaoundé, Cameroun

<sup>2</sup> Geo-Ocean, CNRS, Ifremer, UMR6538, Univ Brest, 29280 Plouzane, France

<sup>3</sup> Département Des Sciences de La Terre, Faculté Des Sciences, Université de Douala, Douala, Cameroun

<sup>4</sup> Department of Geology, Higher Teacher Training College, University of Bamenda, Bambili, Bamenda, Cameroon

<sup>5</sup> Département de Séismologie et Géologie, Observatoire Volcanologique de Goma-RDC, Goma, République Démocratique du Congo

## 1 Introduction

The Cameroon Volcanic Line (CVL) is an alignment of volcanoes stretching over a distance of 1700 km (Njome and De Wit 2014) from the Atlantic Ocean (Gulf of Guinea) to mainland Africa. The CVL is divided into three segments: the oceanic sector (Annobon, São Tomé, and Príncipe), the continental/oceanic boundary (c.o.b.: Bioko, Etinde, and Mount Cameroon), and the purely continental sector. This last part of the CVL is marked by a trend of large massifs including the Manengouba, Bamouto, Bamenda, and Oku mountains (Kamgang et al. 2010, 2013). The volcanic activity developed from the upper Cretaceous ( $68.8 \pm 1.7$  Ma, Ngonge et al. 2014) to present with the eruptions of Mount Cameroon of March–April 1999 and May–July 2000 (Suh et al. 2003). CVL lavas are typically characterized by alkaline (Marzoli et al. 2000; Kamgang et al. 2013; Pouplet et al. 2014; Merle et al. 2017; Gountié Dedzo et al. 2019), transitional (Fosso et al. 2005; Kuepouo et al. 2006; Moundi et al. 2007; Okomo Atouba et al. 2016; Ziem à Bidias et al. 2018; Lemdjou et al. 2020), and rare tholeiitic rocks (Ngounouno et al. 2001). The above studies support the evolution of silicic lavas by fractional crystallization of the mafic melts, accompanied by crustal contamination. This contamination has been demonstrated by Kamgang et al. (2013) in Mount Bamenda and by Tchuimegnie Ngongang et al. (2015) in the Bafang volcanic area. Concerning the origin of the magmas, several detailed investigations of the petrography and geochemistry of volcanic rocks have been carried out to understand the source of lavas of the CVL and their evolutions. Several hypotheses have been suggested: Halliday et al. (1988, 1990) proposed the destruction of the lithosphere and the impregnation of the uppermost mantle by the St. Helena hot spot during the formation of the South Atlantic Ocean. This mantle was subsequently melted to form the Cameroon line which appears to be derived from a rising hot zone initiated by the early plume activity; for Lee et al. (1994), the Cameroon Line originates from a sublithospheric enriched “hot zone” periodically fed by melted deep mantle plumes, and this zone of hotter mantle represents reactivated mantle previously enriched during the opening of the South Atlantic in the Mesozoic. Marzoli et al. (1999) concluded that the Cameroon volcanic line as a whole may not be interpreted as the surface expression of simple hotspot magmatism, confirming earlier conclusions of Fitton and Dunlop (1985) and Fitton (1987), drawn from a more restricted database. However, certain recent geological data also show that the lavas of the CVL do not have the same mantle sources as the St. Helena mantle plume, suggesting that the plume is not the source of the CVL (Marzoli et al. 2000;

Rankenburg et al. 2005; Yokoyama et al. 2007; Tchuimegnie Ngongang et al. 2015; Merle et al. 2017; Ziem à Bidias et al. 2018; Lemdjou et al. 2020). In other hypotheses, the development of volcanism has been linked to several hotspots (Ngounouno et al. 2003; Ngako et al. 2006; Dérulette et al. 2007) or tectonics and small-scale convection in the upper mantle at the base of the lithosphere (King and Ritsema 2000; Reusch et al. 2011; De Plaein et al. 2014; Adams et al. 2015).

To contribute to this debate, we perform a detailed study of volcanic rocks of the Bafoussam area, located within the Western Cameroon highlands in the central part of the CVL (Fig. 1a and b). This zone is bounded by Mount Bamouto to the North-West, Mount Bangou to the South, Bamoun plateau to the East, and Bafang volcanic area to the South-West which shows that the volcanic activity was very important in this region. The previous geologic studies on volcanism were focused on the above-mentioned volcanic edifices, thus leaving large surfaces of lava plateau without detailed geologic data. This study presents petrographic, mineral, and whole-rock chemical data, K–Ar ages, and Sr–Pb–Hf isotopes on some volcanic rocks from the Bafoussam area.

## 2 Geological setting and previous work

The Bafoussam volcanic area is located within the Western Cameroon Highlands in the central part of the CVL. It is dominated by fissural volcanism and exhibits volcanic lava outcrops called “plateau basalt”. These outcrops occur in a vertical or inclined prism, blocks and balls clustered or scattered and result from partly eroded lava flows. The lavas sampled in this area are mafic, intermediate, and felsic. The volcanic rocks lie on a Pan-African (650 Ma) granitoids discontinuous basement (Djouka-Fonkwe et al. 2008). The previous works based on macroscopic descriptions show that this area is composed of aphyric or porphyritic basalts and andesites (Dumort 1968; Tchoua 1974). However, many volcanic studies have been carried out in some neighbouring localities like Bangou (Fosso et al. 2005), Bana (Kuepouo et al. 2006), Bafang (Tchuimegnie Ngongang et al. 2015), Bamoun plateau (Moundi et al. 2007; Okomo Atouba et al. 2016; Ziem à Bidias et al. 2018), the eastern edge of the West Cameroon Highlands (Lemdjou et al. 2020) and Fotouni (Ngongang Tchikankou et al. 2020). According to these authors, the lavas are mafic and intermediate and are of transitional and alkaline affinity.

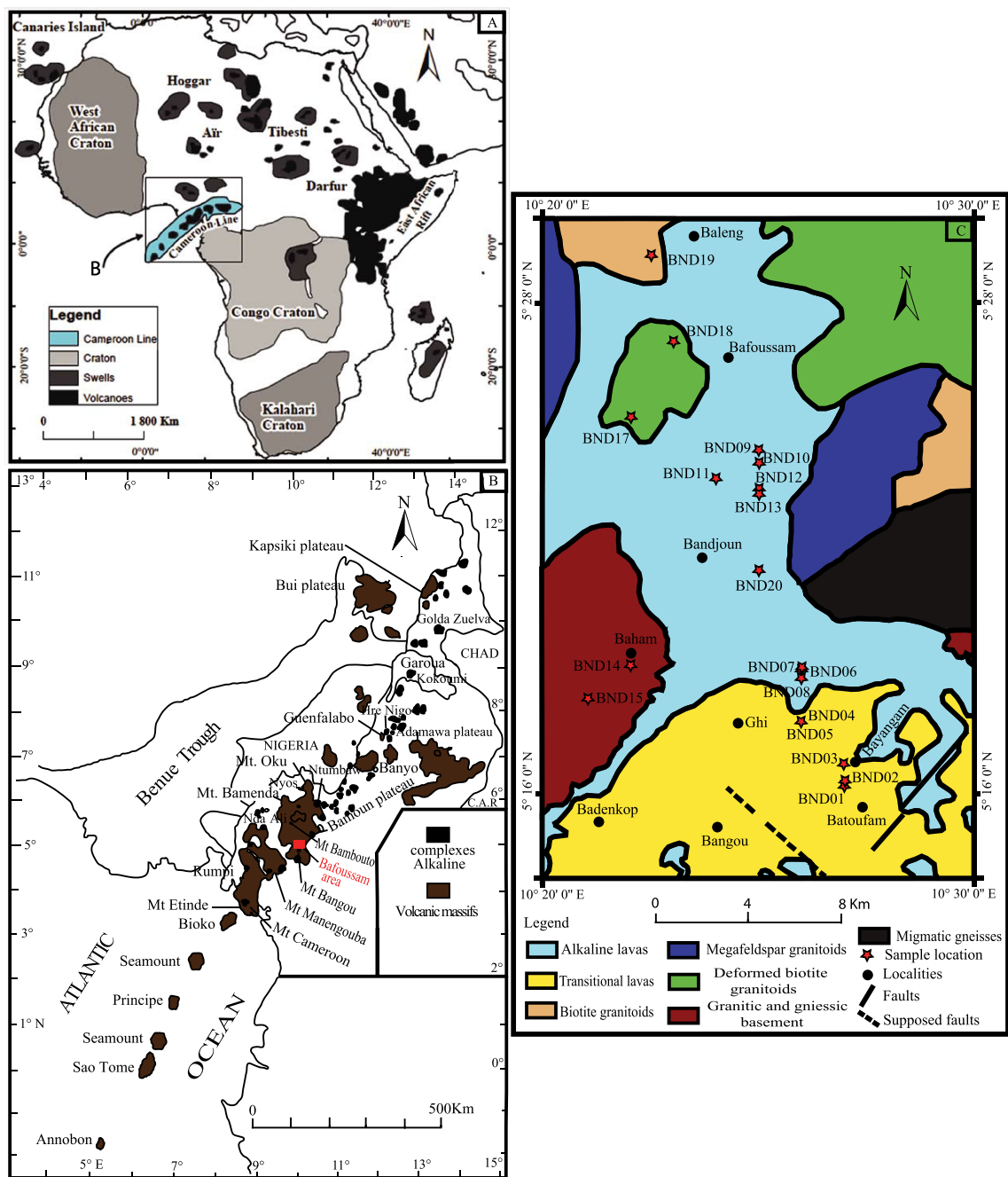


**Fig. 1** **a** Location map of the Cameroon Volcanic Line; the main geologic features of Africa are indicated. **b** Generalized map of the Cameroon Volcanic Line (Halliday et al. 1988), with the location of the Bafoussam volcanic area. Orientation of seamounts after Burke (2001). **c** Simplified geological map of the studied area and location of the samples

### 3 Analytical methods

#### 3.1 K–Ar geochronology

Potassium–argon ages were measured at the Université de Bretagne Occidentale, in Brest (France) on chips of whole rock lavas, 0.3–0.15 mm in size, that were prepared after crushing and subsequent sieving of the solid samples. The preparation and analysis methods are the same as described in Tchuimegnie Ngongang et al. (2015). Isotopic dilution was performed using the method described in Bellon et al. (1981).

#### 3.2 Major and trace element analyses

Whole-rock major elements were measured on the Horiba-Jobin–Yvon® Ultima 2 ICP-AES at the IUEM (European Institute for Marine Studies, Brest, France). A detailed description of the analytical procedure is given in Cotten et al. (1995) and the data presented here were obtained using the same methods as described in Tchuimegnie Ngongang et al. (2015).

Trace element concentrations were measured with a Thermo Element 2 HR-ICP-MS in Brest (France), with the same procedure as described in Tchuimegnie Ngongang et al. (2015).

#### 3.3 Sr-Pb-Hf isotopic analyses

Pb and Hf isotope compositions were analyzed using the Thermo Neptune MC-ICP-MS of IUEM (Brest) and Sr isotopic measurements were performed on a Thermo Scientific Triton in the same laboratory.  $2\sigma$  internal errors never exceeded the last significant digit ( $1E^{-5}$ ) in each analysis. All the analytical parameters are identical to those described in Tchuimegnie Ngongang et al. (2015).

### 4 Nomenclature and petrography

#### 4.1 Nomenclature

All major-element compositions were recalculated to 100% on an anhydrous basis. The Bafoussam volcanic rocks have been classified using the TAS diagram (Le Bas et al. 1986; Fig. 2a) with the alkaline–subalcaline dividing line of Irvine and Baragar (1971). According to this diagram, the samples plot in basanite, hawaiite, basalt, basaltic andesite, and trachyte fields. A clear two groups compositional distribution in terms of  $\text{SiO}_2$  content is observed: mafic (45.7–52.6 wt.%) and felsic (63.6–63.8 wt.%) groups. In the  $\text{Na}_2\text{O}$  vs.  $\text{K}_2\text{O}$  diagram of Middlemost (1975) shown in

Fig. 2b, all the mafic lavas plot in the Na-series field ( $\text{Na}_2\text{O}/\text{K}_2\text{O} = 2.10\text{--}4.46$ ).

#### 4.2 Petrography

The Bafoussam lavas include mafic and felsic rocks, which can be divided into three groups according to their mineral assemblage and magmatic affinity: mafic alkaline lavas (basanite, hawaiite, and basalt), mafic transitional lavas (basalt and basaltic andesite) and felsic transitional lavas (trachyte).

Mafic alkaline lavas usually have microlitic porphyritic textures (Fig. 3a and b). They contain plagioclase, clinopyroxene, olivine, and Fe-Ti oxides as microlites, with fluidal texture. Plagioclase and clinopyroxene and rare olivine microcrysts and phenocrysts are scattered in the groundmass.

Mafic transitional lavas have microlitic porphyritic or microlitic aphyric texture with a fluidal tendency (Fig. 3c). Their mineral assemblage remains constant. The plagioclases, pyroxenes, and opaque minerals constitute the essence of the phenocrysts. Olivine is absent or occasional. The mineral assemblage of basaltic andesite is almost identical to that of transitional basalts. Nevertheless, it is slightly more differentiated.

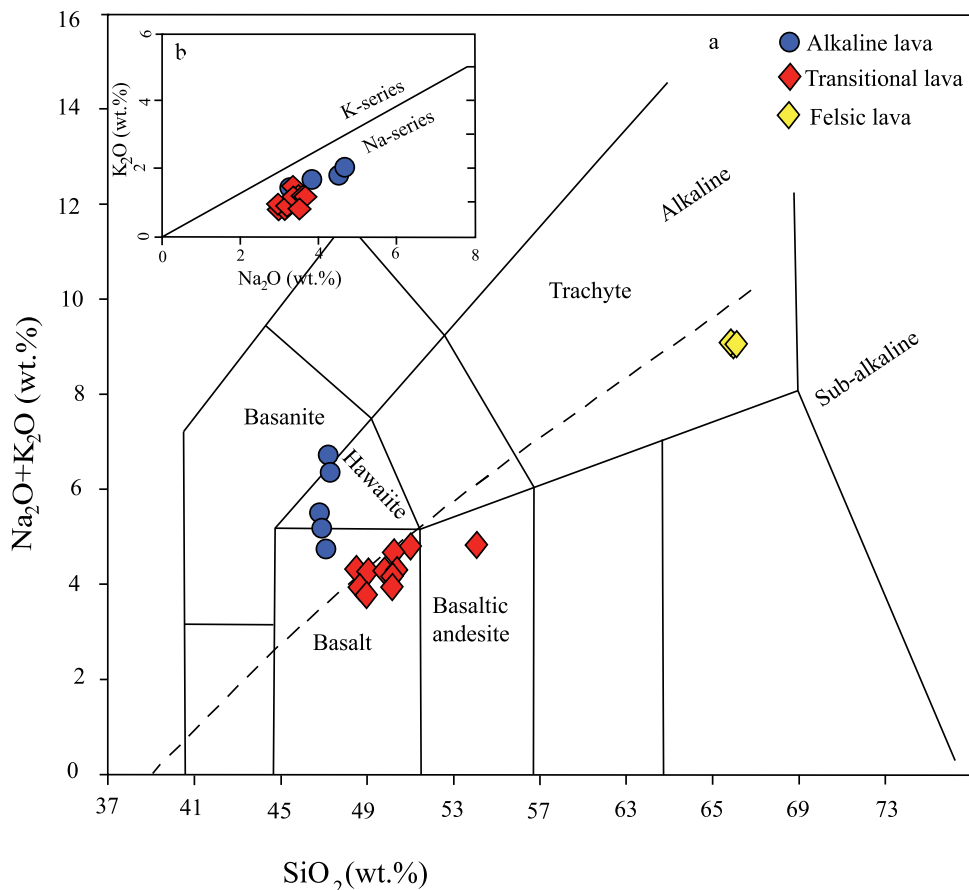
Felsic transitional lavas have a microlitic fluidal or trachytic texture (Fig. 3d). The microscopic characteristic shows that the trachytes are dominated by microlites and phenocrysts of sanidine. The other representative minerals are microlites of feldspar and microphenocrysts of oxides, pyroxene, and quartz.

### 5 Mineral chemistry

#### 5.1 Olivine

Olivine is present in the alkaline lavas as phenocryst, microphenocryst, and microlite and rare/or absent in the transitional lavas. Representative microprobe analyses of olivines are given in Supplementary Material. The chemical composition has a range that evolves from forsterite-rich ( $\text{Fo}_{71.2}$ ) to forsterite-poor ( $\text{Fo}_{49.1}$ ) olivine. Olivine in alkaline basalt ( $\text{Fo}_{64.9\text{--}71.2}$ ), basanite ( $\text{Fo}_{65.1\text{--}70.9}$ ), and hawaiite ( $\text{Fo}_{65.5\text{--}66.5}$ ) have the highest forsterite content. It is more Fe-rich in the transitional basaltic andesite ( $\text{Fo}_{67.4\text{--}49.1}$ ). The high  $\text{CaO}$  contents ( $> 0.18$  wt.%) (except for one analysis in olivine of alkaline lavas) reflect low pressures of crystallization, typical of crustal conditions (Köhler and Brey 1990; Hirschmann and Ghiorso 1994) and higher than that of peridotites ( $< 0.1$  wt.%, Simkin and Smith 1970).  $\text{CaO}$  and  $\text{NiO}$  concentrations in the alkaline lava olivines are generally higher than those in transitional

**Fig. 2** **a** Total Alkalies vs. Silica diagram (Le Bas et al. 1986) for the Bafoussam lavas. The dotted line is from Irvine and Baragar (1971). **b**  $\text{Na}_2\text{O}$  vs.  $\text{K}_2\text{O}$  subdivision diagram of K- and Na-series of mafic lavas (Middlemost 1975). In these diagrams and in all the following dealing with major and trace elements as well as isotopic ratios, analytical uncertainties are lower than the symbol size



lavas. MnO contents are very low in almost all types of lavas, except for three points of analyses of alkaline basalt.

## 5.2 Pyroxene

Representative analyses of pyroxenes are listed in Supplementary Material. In the Wo-En-Fs classification diagram of Morimoto et al. (1988), the pyroxene of the two groups of rocks (alkaline and transitional) are mainly diopside, augite with minor pigeonite and clinoenstatite (Fig. 4a). The clinopyroxenes of alkaline lavas plot in the augite and diopside fields. The wollastonite content is higher in diopside ( $\text{Wo}_{45.3-48.3}\text{En}_{35.9-40.7}\text{Fs}_{12.4-15.6}$ ) than in augite ( $\text{Wo}_{39.7-44.8}\text{En}_{39.4-48.5}\text{Fs}_{11.7-15.9}$ ). The clinopyroxenes of the transitional lavas plot in the augite field and have low wollastonite content ( $\text{Wo}_{37.2-42.6}\text{En}_{35.3-40.9}\text{Fs}_{18.7-26.2}$ ). Orthopyroxenes are only found in the transitional lavas ( $\text{Wo}_{4.5-4.8}\text{En}_{39.3-65.5}\text{Fs}_{29.9-45.7}$ ) and are sometimes associated with pigeonite. Their geochemical composition is very variable in MgO (13.36–23.78 wt.%) and FeO (19.34–28.85 wt.%). They are low in CaO (2.28–7.03 wt.%) and Na<sub>2</sub>O (0.05–0.15 wt.%). The unique analysis of pigeonite is poor in Mn (0.86 wt% MnO) compared to

those described in the Mbabo volcano massif of the CVL (3.3–3.6 wt% MnO; Bardintzeff et al. 2020).

Diopside ( $\text{CaMgSi}_2\text{O}_6$ ) is the simplest clinopyroxene structural formula, where Ca occupies the M2 site, Mg is in the octahedral M1 site and Si is tetrahedrally coordinated. Substitution of divalent cations Fe, Mn, and Mg for Ca in the M2 site and Fe and Mn for Mg in the M1 site produces the compositional variations observed in the pyroxene quadrilateral (Farahat et al. 2006). However, almost all pyroxene analyses of the alkaline lavas contain an excess of aluminum after allocation of Al to the tetrahedral site, contrarily of transitional lavas (Fig. 4b). Titanium contents are positively correlated with Mg# (Fig. 4c). According to Binns et al. (1970), the Al and Ti contents of calcic-pyroxene reflect the silica activity of the magma and the crystallization conditions, with high Al and Ti contents being associated with low Si activities and elevated pressures. Accordingly, the relatively high Al and Ti contents of pyroxene from most of the alkaline lavas, reflect their crystallization at relatively high pressure and low silica activity compared to those from transitional lavas. It is of petrological importance to note the significant difference in the Si, Al, Ti, Na, and Mg# =  $[100 * \text{Mg}/(\text{Mg} + \text{Fe}^{2+})]$  between pyroxenes of the two groups of lavas (alkaline and

**Fig. 3** Photomicrographs of thin sections of mafic and felsic lavas from the Bafoussam area. **a** and **b** Microlitic porphyritic texture of alkaline lavas (hawaiite and basanite, respectively). **c** Microlitic aphyric texture with the fluidal tendency in a transitional basalt. **d** Trachytic texture with microlites and phenocrysts of sanidine in transitional trachyte. Cpx = clinopyroxene, Pl = plagioclase, Ol = olivine, Sa = sanidine and Op = opaque mineral

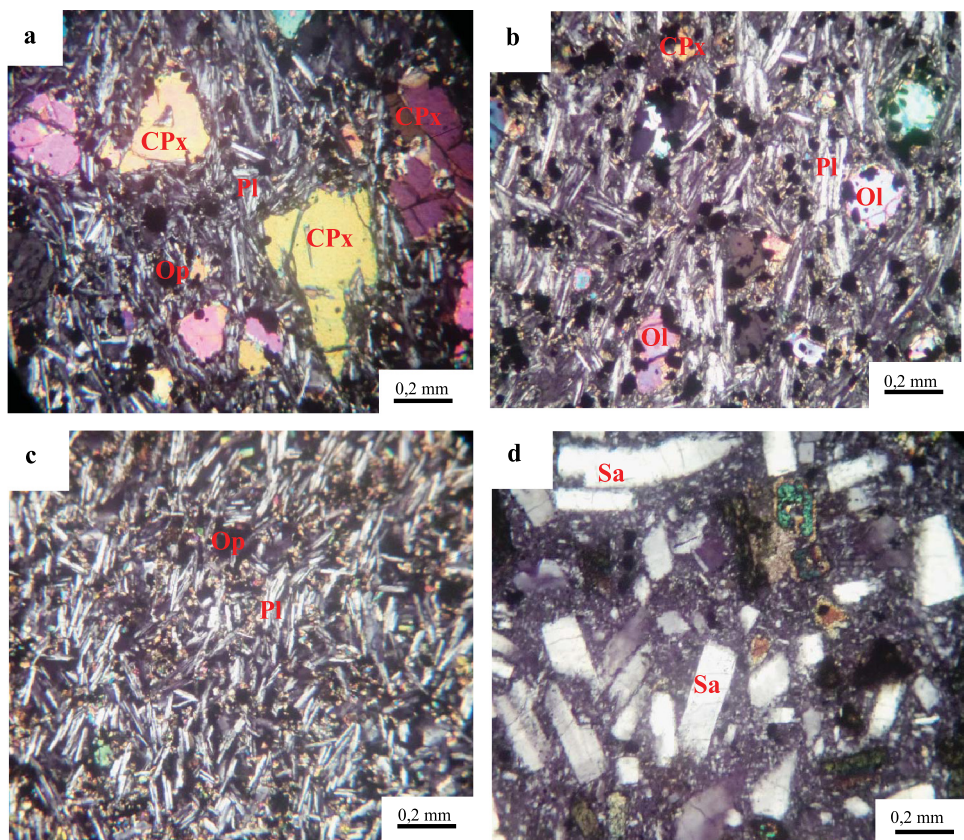
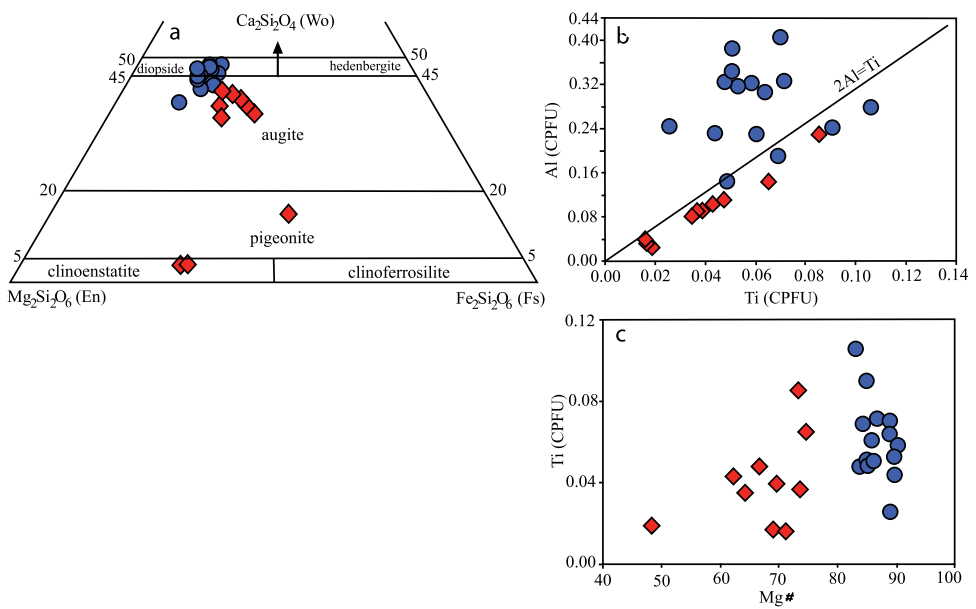


**Fig. 4** (a) Compositions of pyroxenes plotted in the atomic Mg-Fe-Ca ternary diagram (boundaries after Morimoto et al., 1988). **b** and **c** Cation variations in pyroxenes. CPFU = cation per formula unit. Legend in Fig. 2



transitional). Pyroxenes of the alkaline lavas have higher values in Al, Ti, Na, and Mg# compared to those of transitional lavas.

### 5.3 Feldspar

Feldspar represents the main mineral phase in the Bafoussam lavas. Their compositions are shown in Supplementary Material. These feldspars evolve in two different series: plagioclase and alkali feldspar. The

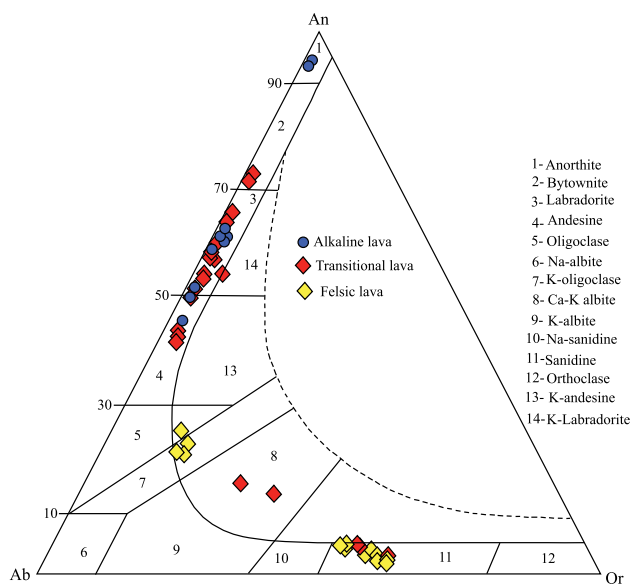


**Fig. 5** Nomenclature of feldspars (Smith and Brown, 1988) analyzed in the transitional and alkaline rocks

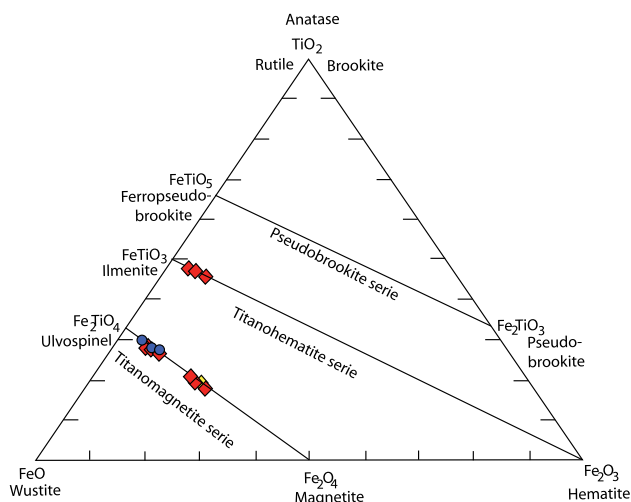


**Fig. 6 a** Chemical composition of Fe-Ti oxide minerals in the Bafoussam lavas. Legend in Fig. 2

plagioclases range from andesine to anorthite compositions in the alkaline lavas ( $\text{An}_{46.9-51.1}-\text{An}_{94.0-94.3}$  respectively) and from andesine to bytownite ( $\text{An}_{43.1-44.8}-\text{An}_{73.2-74.4}$  respectively) in the transitional lavas but are mainly labradorite in the two groups (Fig. 5). Alkali feldspars occur in the transitional and felsic lavas. Their composition ranges from sanidine to Ca-K-albite in the transitional lavas ( $\text{An}_{3-6}-\text{An}_{14}$  respectively) and from sanidine to K-oligoclase ( $\text{An}_{3-5}-\text{An}_{22-24}$  respectively) in the felsic lavas.

## 5.4 Fe-Ti oxide

Representative analyses of Fe-Ti oxides are listed in Supplementary Material. The ternary plot of  $\text{TiO}_2-\text{FeO}-\text{Fe}_2\text{O}_3$  shows ilmenite-hematite and magnetite-ulvöspinel trend evolutions (Buddington and Lindsley 1964; Fig. 6). These Fe-Ti oxides comprise mainly titanomagnetite and ilmenite occurring as groundmass microlites. The ilmenites have a low composition in hematite ( $\text{Fe}_2\text{O}_3$ ) in solid solution ( $\text{Ilm}_{97.2-96.2}\text{Hem}_{3.7-2.7}$ ). Magnetite occurs as Ti-magnetite with high contents of ulvöspinel end-member ( $\text{Fe}_2\text{TiO}_4$ ) and very low in magnesioferrite ( $\text{MgFe}_2\text{O}_4$ ) end-members in transitional and felsic lavas, and Ti-magnetite rich in the ulvöspinel end-member in alkaline lavas. The chemical compositions of Usp-Mt vary from basanites ( $\text{Usp}_{76.6}\text{Mt}_{23.3}$ ) to hawaiites ( $\text{Usp}_{82.5-79.3}\text{Mt}_{20.6-17.4}$ ) in the alkaline lavas. In the transitional lavas, these compositions show a large variation ( $\text{Usp}_{73.7-46.7}\text{Mt}_{53.2-26.2}$ ). Only one analysis was carried out in the trachytes and it has a chemical composition of  $\text{Usp}_{49.4}\text{Mt}_{50.5}$ .

## 6 Whole-rock geochemistry

### 6.1 Major and trace elements

The major and trace element contents of the rocks are presented in Table 1. The compositions of the various oxides were recalculated to 100% based on a hydrous-free basis. The samples show a range in  $\text{SiO}_2$  from 45.7 to 63.8 wt% but there is a gap in the silica content with no intermediate lavas. The mafic lavas have alkaline and transitional affinity and the felsic lavas are transitional. The Mg-number values ( $100 \times \text{Mg}/(\text{Mg} + \text{Fe})$  in mol), assuming  $\text{FeOt} = \text{Fe}_2\text{O}_3 * 0.8998$ ) vary from 39.8 to 50.1 in mafic alkaline, from 20.4 to 39.3 in mafic transitional and from 2.7 to 3.2 in felsic transitional lavas. Alkaline lavas are nepheline and olivine normative, whereas transitional lavas (mafic and felsic) are hypersthene and quartz normative (Table 1). The major element variations with respect to Th content are illustrated in Fig. 7. Negative correlations of  $\text{MgO}$  and  $\text{CaO}$  with Th and positive correlations of  $\text{K}_2\text{O}$  with Th suggest variable degrees of fractional crystallization as the main evolutionary process for the mafic transitional and alkaline lavas. In the  $\text{Al}_2\text{O}_3$  vs. Th diagram, we observe an almost constant evolution between some samples of the alkaline and transitional mafic lavas; this indicates that there was no plagioclase fractionation in both groups of lavas. However, some samples from the transitional mafic lavas have low and almost similar  $\text{Al}_2\text{O}_3$  contents to the felsic lavas, suggesting that a contaminant that was poor in  $\text{Al}_2\text{O}_3$  diluted its concentration in these lavas.

**Table 1** Major (wt. %) and trace (ppm) element concentrations and normative composition for the Bafoussam lavas

Samples	Transitional lavas									
	Basalt									
	BND01	BND03	BND04	BND05	BND06	BND07	BND08	BND14	BND18	BND20
SiO <sub>2</sub>	47.50	47.20	48.50	48.80	50.30	49.60	48.50	49.20	49.53	47.73
TiO <sub>2</sub>	4.06	3.36	3.97	2.76	2.62	2.87	3.61	2.80	3.07	4.08
Al <sub>2</sub> O <sub>3</sub>	12.70	15.10	13.60	16.00	12.70	16.00	13.10	16.10	12.81	15.60
Fe <sub>2</sub> O <sub>3</sub>	15.00	13.00	14.80	12.20	16.70	12.30	14.60	12.20	15.20	15.62
MnO	0.26	0.13	0.20	0.17	0.41	0.18	0.19	0.18	0.24	0.21
MgO	4.07	4.70	4.21	3.74	2.55	3.84	4.02	3.90	3.65	4.36
CaO	8.74	8.74	8.59	9.29	7.36	8.88	8.11	9.05	7.60	8.45
Na <sub>2</sub> O	3.45	2.91	3.24	3.08	3.60	3.28	3.18	3.19	3.45	2.94
K <sub>2</sub> O	0.77	0.73	0.96	0.74	1.13	0.96	0.99	0.87	1.15	0.92
P <sub>2</sub> O <sub>5</sub>	1.07	0.39	0.57	0.37	1.06	0.45	0.85	0.44	1.63	0.56
LOI	0.99	2.99	0.47	1.89	1.14	1.28	2.11	1.15	0.98	1.36
Total	98.65	99.27	99.08	98.95	99.54	99.66	99.38	99.11	99.33	99.24
Mg#	31.30	37.86	32.41	34.08	20.40	34.51	31.64	34.99	28.81	31.99
Quartz	—	—	—	0.63	1.74	0.16	1.28	0.15	2.00	0.28
Orthose	4.65	4.47	5.74	4.49	6.77	5.76	6.01	5.24	6.91	5.54
Albite	29.84	25.53	27.74	26.78	30.88	28.17	27.64	27.52	29.59	25.40
Anorthite	17.27	26.94	19.96	28.41	15.36	26.49	19.05	27.57	16.31	19.91
Nepheline	—	—	—	—	—	—	—	—	—	—
Diopside	16.73	12.80	16.25	13.86	12.60	12.80	13.95	12.82	9.41	16.03
Hypersthene	16.49	18.73	17.57	17.17	21.89	17.64	20.13	17.86	23.05	20.57
Olivine	1.65	1.38	0.90	—	—	—	—	—	—	—
Magnetite	2.94	2.58	2.87	2.40	3.24	2.39	2.87	2.38	2.96	3.05
Ilmenite	7.88	6.62	7.63	5.39	5.04	5.53	7.04	5.42	5.92	7.90
Apatite	2.54	0.94	1.35	0.86	2.48	1.05	2.02	1.03	3.84	1.33
Li	3.79	3.95	4.87	3.67	5.29	5.48	6.3	6.16	6.88	5.12
Be	1.02	0.763	1.14	0.954	1.4	1.25	1.28	1.2	1.61	1.09
Sc	27.6	6.96	24.4	18.5	31.4	22.6	25.5	22.3	22.4	27.5
V	239	280	288	236	72.7	231	248	231	119	324
Cr	6.56	60.2	6.4	45.2	7.76	45.5	16.9	39.8	5.58	11.6
Co	37.3	49.3	40.2	39.6	17	37.8	39.5	34.1	26.6	44.4
Ni	7.58	43.4	4.91	39.1	4.79	29.8	14.6	34.8	2.06	16.1
Cu	50.1	60.9	46	65.9	33.6	56.6	43	54.5	32.4	50.3
Zn	152	131	145	112	164	120	142	116	150	154
Ga	24.2	22	23.4	21.7	26.6	23.9	24.1	22.5	24.7	23.3
Ge	2.61	1.78	2.37	1.96	3.06	2.25	2.58	1.97	2.54	2.47
Rb	14	3.98	12.9	15.5	24	11.5	25.3	12.4	20.6	26.9
Sr	466	330	423	409	482	471	473	458	460	434
Y	38.6	9.13	28.9	20	46.6	30.9	37.3	27.2	50.8	33.6
Zr	209	153	229	191	257	237	234	201	268	218
Nb	24.8	19.7	29.1	24.4	31.7	29.2	23.3	26.9	28.8	24.1
Ba	299	187	262	203	373	240	426	238	382	287
La	24.5	8.93	21.4	16.7	30.7	23	26.9	21.3	39.2	23.8
Ce	58.8	21.5	49.8	35	74.4	51.7	63.1	46.6	93.5	50.4
Pr	8.49	2.85	6.73	4.75	10.6	6.77	8.53	6.09	12.6	6.84
Nd	39.6	13.3	29.9	21.1	49.3	29.4	38.4	26.5	57.1	31
Sm	9.74	3.2	7.11	5.07	12	6.99	9.23	6.21	13.5	7.62

**Table 1** continued

Samples	Transitional lavas									
	Basalt									
	BND01	BND03	BND04	BND05	BND06	BND07	BND08	BND14	BND18	BND20
Eu	3.82	1.24	2.47	1.74	5.33	2.37	3.46	2.08	4.53	2.8
Gd	10.2	3.23	7.35	5.12	12.2	7.15	9.38	6.31	13.6	7.88
Tb	1.48	0.483	1.1	0.756	1.74	1.07	1.35	0.951	1.91	1.16
Dy	8.17	2.67	6.12	4.2	9.64	6.05	7.52	5.38	10.3	6.54
Ho	1.48	0.499	1.13	0.773	1.74	1.13	1.37	0.993	1.85	1.21
Er	3.74	1.28	2.92	2	4.43	2.95	3.49	2.59	4.62	3.14
Tm	0.476	0.167	0.386	0.264	0.571	0.386	0.455	0.342	0.581	0.406
Yb	2.89	0.967	2.37	1.61	3.53	2.39	2.69	2.1	3.46	2.46
Lu	0.404	0.131	0.33	0.227	0.519	0.339	0.378	0.297	0.484	0.346
Hf	4.84	3.46	5.22	4.37	5.77	5.35	5.31	4.78	6.4	4.98
Ta	1.53	1.19	1.76	1.43	1.83	1.71	1.44	1.64	1.79	1.45
Pb	1.89	1.22	2.53	2.07	2.38	2.23	3.19	2.11	3.69	2.34
Th	1.82	0.405	2.36	1.73	2.4	2.47	2.94	2.18	3.61	2.11
U	0.552	0.381	0.644	0.495	0.731	0.649	0.709	0.602	0.957	0.546
Eu/Eu*	1.21	1.22	1.08	1.08	1.39	1.06	1.18	1.05	1.06	1.14
	Alkaline lavas									
Samples	Basalt		Basanite		Hawaiite		Felsic lavas			
	BND15	BND09	BND10	BND17	BND19	Trachyte	BND11	BND12	BND13	
SiO <sub>2</sub>	46.10	46.34	46.35	46.30	45.68	63.73	63.64	63.77		
TiO <sub>2</sub>	2.72	2.91	2.93	2.84	2.83	0.35	0.36	0.36		
Al <sub>2</sub> O <sub>3</sub>	15.30	16.57	16.36	15.57	15.52	13.80	13.99	13.97		
Fe <sub>2</sub> O <sub>3</sub>	12.00	12.47	12.49	12.38	12.88	6.97	7.21	7.19		
MnO	0.19	0.20	0.21	0.21	0.21	0.15	0.12	0.12		
MgO	7.17	4.89	5.18	6.25	5.76	0.12	0.14	0.12		
CaO	8.87	7.39	7.39	9.21	8.69	2.27	2.31	2.20		
Na <sub>2</sub> O	3.26	4.60	4.44	3.81	3.43	3.34	3.58	3.55		
K <sub>2</sub> O	1.36	2.00	1.76	1.64	1.63	5.38	5.29	5.17		
P <sub>2</sub> O <sub>5</sub>	0.79	0.74	0.75	0.67	0.70	0.08	0.09	0.08		
LOI	0.94	1.21	0.78	0.23	0.49	1.90	1.39	1.69		
Total	98.73	99.30	98.63	99.10	97.80	98.09	98.14	98.22		
Mg#	50.09	39.77	41.10	45.94	42.96	2.75	3.24	2.70		
Quartz	–	–	–	–	–	16.10	14.73	15.61		
Orthose	8.21	12.00	10.60	9.79	9.88	33.01	32.24	31.60		
Albite	24.47	23.41	25.56	20.07	22.78	29.38	31.29	31.10		
Anorthite	23.59	19.03	19.90	20.75	22.70	7.00	6.69	7.13		
Nepheline	2.00	8.76	6.93	6.75	3.78	–	–	–		
Diopside	13.17	11.12	10.39	17.31	13.94	3.65	4.03	3.18		
Hypersthene	–	–	–	–	–	8.00	8.07	8.46		
Olivine	19.05	15.90	16.73	15.94	17.22	–	–	–		
Magnetite	2.35	2.43	2.44	2.39	2.53	1.96	2.02	2.02		
Ilmenite	5.28	5.62	5.68	5.44	5.51	0.68	0.71	0.70		
Apatite	1.88	1.74	1.77	1.56	1.66	0.20	0.21	0.20		
Li	6.76	11.8	10.9	8.27	8.56	9.66	14.9	12.5		
Be	1.78	2.97	2.92	2.41	2.31	3.64	3.81	3.03		
Sc	20.6	16.6	16.6	20.8	18.3	4.19	5.24	1.88		

**Table 1** continued

Samples	Alkaline lavas					Felsic lavas		
	Basalt		Basanite		Hawaiite	Trachyte		
	BND15	BND09	BND10	BND17	BND19	BND11	BND12	BND13
V	195	173	173	211	181	1.49	1.52	1.87
Cr	189	24.6	36	136	107	9.16	6.07	7.67
Co	42.1	37.4	38.1	42.8	38.6	0.624	0.763	0.728
Ni	116	36.1	40.6	88.9	68.8	0.556	0.402	0.525
Cu	71	47.3	47	75.1	59.9	6.53	6.77	6.51
Zn	116	123	123	134	121	178	141	114
Ga	21.6	24.4	24.6	23.3	23.2	31.8	33.4	26.3
Ge	2.12	2.59	2.56	2.16	2.24	2.19	2.6	1.45
Rb	29.2	47.5	43.5	38.2	37.2	110	107	82.6
Sr	754	817	897	757	812	67.9	62.7	44.1
Y	29.5	36.4	35.3	30.7	31.5	33.6	35.9	13.4
Zr	258	369	350	300	324	402	276	216
Nb	53	66.7	63.4	63.5	68.5	76.3	75.8	72.1
Ba	444	494	480	476	486	874	954	716
La	40.4	54.2	51.8	47.3	50.3	54.3	57.6	11.2
Ce	81.5	107	103	93.8	98.4	127	127	30.2
Pr	9.92	12.9	12.5	11.1	11.7	14	13.7	3.82
Nd	40	49.7	48.5	43.4	45.3	54.5	52	16.5
Sm	8.04	9.57	9.47	8.47	8.76	12	11.4	4.25
Eu	2.64	3.04	3.05	2.79	2.81	2.41	2.42	1.05
Gd	7.7	8.84	8.66	7.92	8.16	10.6	9.75	4.18
Tb	1.11	1.27	1.25	1.15	1.17	1.6	1.47	0.716
Dy	5.99	6.94	6.83	6.28	6.33	8.9	8.21	4.49
Ho	1.07	1.24	1.22	1.11	1.11	1.6	1.46	0.854
Er	2.79	3.31	3.25	2.91	2.94	4.2	3.89	2.31
Tm	0.372	0.45	0.43	0.387	0.388	0.571	0.513	0.322
Yb	2.3	2.79	2.73	2.37	2.39	3.57	3.2	1.96
Lu	0.324	0.403	0.387	0.34	0.34	0.49	0.433	0.272
Hf	5.49	7.85	7.49	6.54	7	11.5	8.95	6.86
Ta	2.97	4.07	3.63	3.7	3.96	4	3.96	3.8
Pb	2.54	3.92	3.78	3.26	3.38	15.5	22.6	10.8
Th	3.88	5.49	5.07	4.85	5.16	8.03	7.92	3.36
U	1.08	1.56	1.46	1.37	1.49	1.71	1.34	0.694
Eu/Eu*	1.06	1.04	1.06	1.08	1.05	0.68	0.73	0.79

(Mg# =  $100 * (\text{MgO}/40.31) / ((\text{MgO}/40.31 + \text{Fe}_2\text{O}_3 * 0.8998) / (71.85 * (1 - 0.15)))$ , with  $\text{FeO}_t = \text{Fe}_2\text{O}_3 * 0.8998$ ; LOI: Loss on ignition;

Eu\* =  $\text{Eu}/(\text{Sm}_n \times \text{Gd}_n)^{1/2}$

The compatible elements show a wide range of Ni and Cr values for an almost constant value of SiO<sub>2</sub> for the alkaline lavas and scattered values for the mafic transitional lavas contrary to the felsic transitional lavas which have very low and constant values. These Ni and Cr values are much lower than 300 and 600 ppm respectively, so the magmas are not primary (Ni: 250–300 ppm and Cr:

500–600 ppm e.g., Green 1976; Kimura and Ariskin 2014). The evolution of incompatible elements shows positive correlations of La, Zr, Nb, and Sr with Th (Fig. 8).

Chondrite-normalized rare earth element (REE) patterns (McDonough 2003) of the Bafoussam samples are enriched in light REE [alkaline lavas ( $\text{La}/\text{Yb}$ )<sub>n</sub> = 11.9–14.3, transitional lavas ( $\text{La}/\text{Yb}$ )<sub>n</sub> = 3.4–7.7 and felsic lavas ( $\text{La}/$

**Fig. 7** Whole rock major element composition (in wt.%) versus Th (in ppm) for the transitional and alkaline rocks

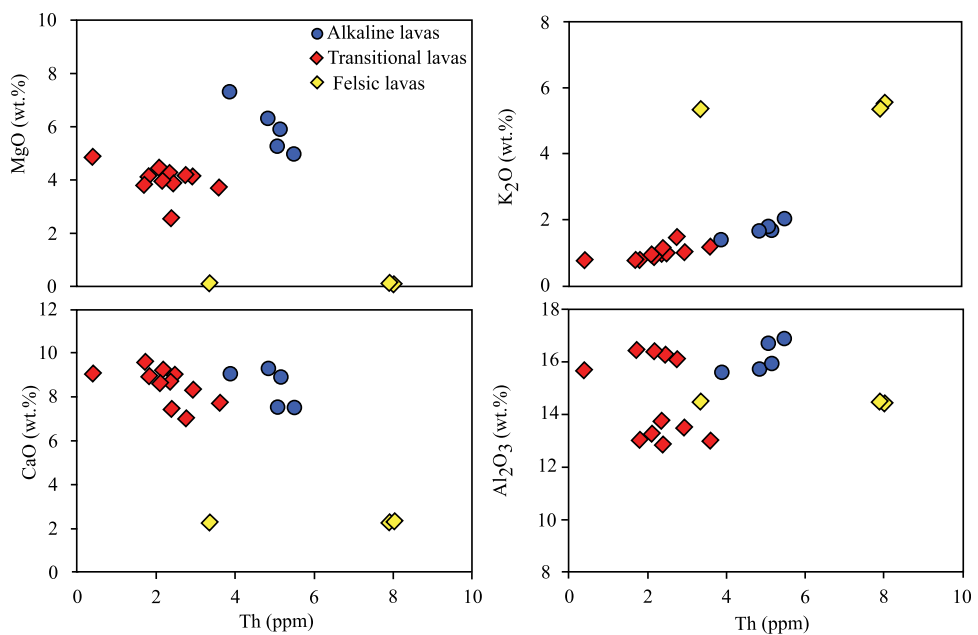
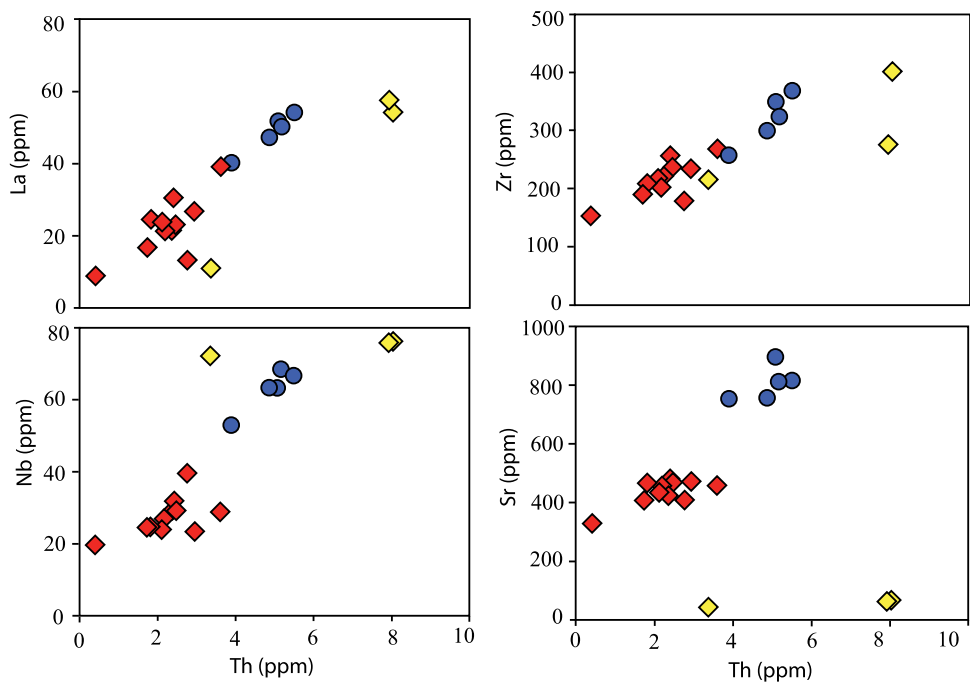


**Fig. 8** Variations of some trace elements (in ppm) versus Th (in ppm). Legend in Fig. 8



$\text{Yb}_n = 3.9\text{--}12.2$ ; where the subscript  $n$  means chondrite-normalized] (Fig. 9a, b and c). These values are higher than those of N-MORB and E-MORB [ $(\text{La/Yb})_n = 0.56$  and 1.81 respectively; Sun and McDonough 1989]. In Fig. 9b, some samples of transitional lavas exhibit weak/or high positive europium anomalies ( $\text{Eu/Eu}^* = 1.05\text{--}1.39$ , where Eu is normalized Eu and  $\text{Eu}^*$  is Eu interpolated between normalized Sm and Gd:  $\text{Eu}^* = \text{Eu}/(\text{Sm}_n \times \text{Gd}_n)^{1/2}$ ). This anomaly is absent in alkaline lavas ( $\text{Eu/Eu}^* = 1.04\text{--}1.08$ ; Fig. 9a). All samples of felsic transitional lavas show

negative europium anomalies ( $\text{Eu/Eu}^* = 0.68\text{--}0.79$ ; Fig. 9c), as evidence of fractional crystallization of feldspar.

The trace element patterns of mafic alkaline and transitional lavas normalized to the primitive mantle (McDonough 2003) share the same OIB-like intraplaque characteristics with enrichment in highly to moderately incompatible trace elements (Fig. 9d and e). All alkaline lavas display highly fractionated patterns with negative K and Pb anomalies, and positive Nb, and Ba anomalies. Transitional lavas exhibit

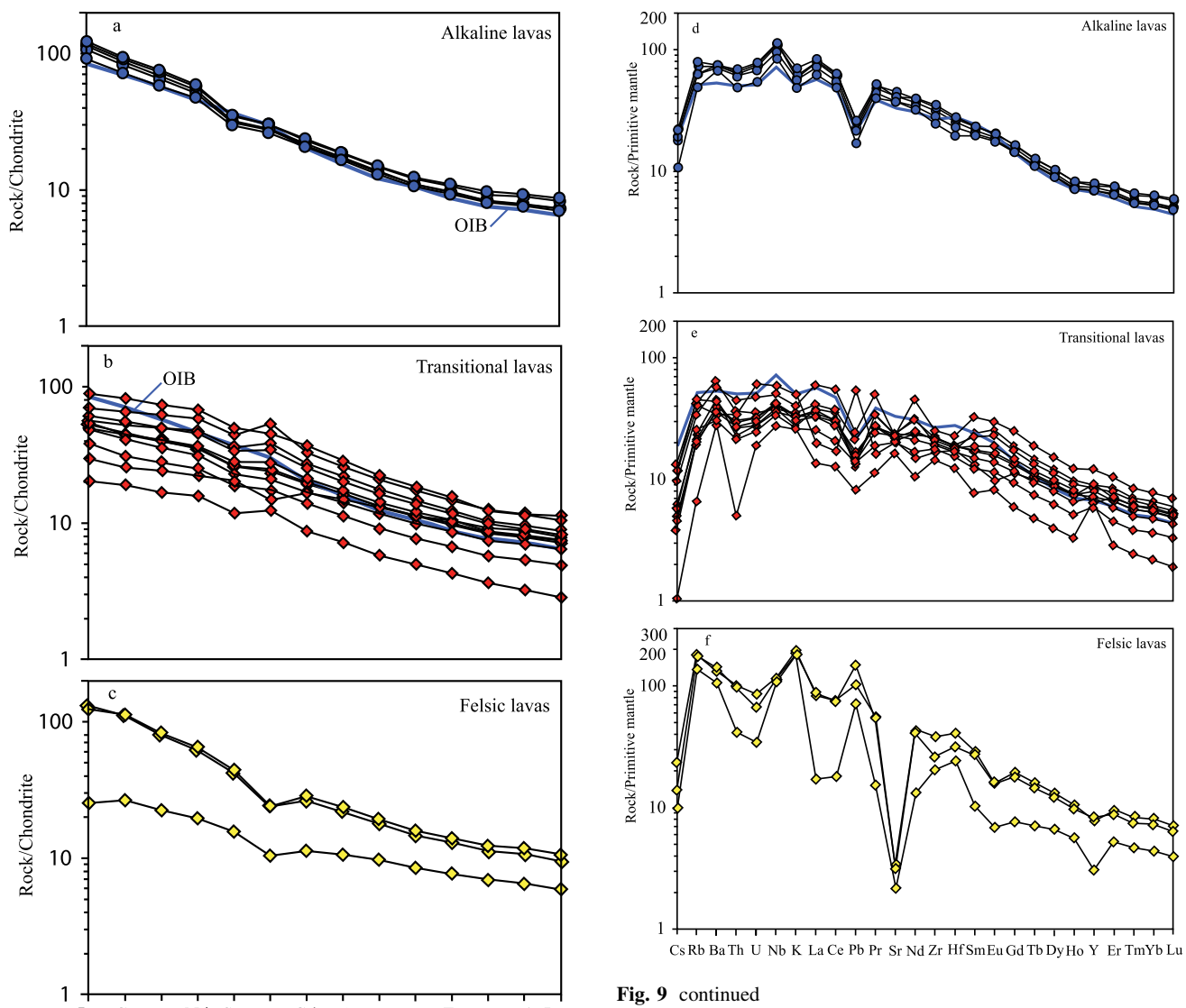


Fig. 9 continued

**Fig. 9 a, b, c** Rare earth element (REE) patterns normalized to chondrite values (McDonough, 2003) for the Bafoussam lavas; **d, e, f** Extended trace element patterns normalized to the composition of the primitive mantle (McDonough 2003). OIB values from Sun and McDonough (1989)

negative Th, K, Pb, Sr, Zr-Hf anomalies and positive Nb, Ba, Eu anomalies. Felsic transitional lavas patterns show positive K, Pb, and Y anomalies and negative Sr, Eu, and Th-U anomalies (Fig. 9f).

## 6.2 Sr, Pb, and Hf isotope geochemistry

The Sr, Pb, and Hf isotopic ratios of five mafic alkalines, eleven mafic transitional, and three felsic transitional samples are listed in Table 2. The initial isotopic ratios ( $^{87}\text{Sr}/^{86}\text{Sr}$ ) have been recalculated at 7 Ma for the mafic alkaline, 41 Ma for the mafic transitional, and 44 Ma for the felsic transitional lavas, for samples that have not been

dated. The other samples have been recalculated with their absolute ages. The values of the initial  $^{87}\text{Sr}/^{86}\text{Sr}$  ratios of alkaline lavas (0.70293–0.70321) are lower than those of mafic transitional (0.70374–0.70536) and felsic transitional (0.70575–0.70703) lavas, and their measured  $^{176}\text{Hf}/^{177}\text{Hf}$  ratios (0.28295–0.28299) are higher than in mafic transitional (0.28278–0.28292) and felsic transitional (0.28257–0.28258) lavas. The  $^{208}\text{Pb}/^{204}\text{Pb}$ ,  $^{207}\text{Pb}/^{204}\text{Pb}$  and  $^{206}\text{Pb}/^{204}\text{Pb}$  ratios of alkaline lavas (39.498–39.917, 15.619–15.655 and 19.785–20.193, respectively) are higher than those of mafic transitional lavas (38.519–39.246, 15.535–15.623 and 17.979–18.991, respectively). Felsic transitional lavas have higher  $^{208}\text{Pb}/^{204}\text{Pb}$  and  $^{207}\text{Pb}/^{204}\text{Pb}$  ratios than the mafic transitional lavas (39.611–39.633, 15.660–15.662, respectively), for similar  $^{206}\text{Pb}/^{204}\text{Pb}$  ratios (18.396–18.401).

In Fig. 10, the variations of  $\text{Sr}_i$  and Pb isotopic compositions of mafic lavas follow the evolution of those of the

**Table 2** Sr, Hf and Pb isotopic compositions of Bafoussam lavas

Samples	Rocks	Hf	$^{186}\text{Hf}/^{187}\text{Hf}$	Error	eHf	$^{87}\text{Sr}/^{86}\text{Sr}$	Error	$(^{87}\text{Sr}/^{86}\text{Sr})\text{i}$	$^{208}\text{Pb}/^{204}\text{Pb}$	$^{207}\text{Pb}/^{204}\text{Pb}$	$^{206}\text{Pb}/^{204}\text{Pb}$
BND01	Transitional basalt	0.28292	0.000003	5.2	0.70417	0.000003	0.70412	38.937	15.586	18.991	
BND03	Transitional basalt	0.28288	0.000003	3.8	0.70425	0.000004	0.70422	38.852	15.571	18.796	
BND04	Transitional basalt	0.28288	0.000003	3.8	0.70432	0.000004	0.70427	39.246	15.618	18.666	
BND05	Transitional basalt	0.28290	0.000003	4.5	0.70381	0.000004	0.70374	39.049	15.613	18.703	
BND06	Transitional basalt	0.28290	0.000003	4.5	0.70472	0.000004	0.70463	38.803	15.578	18.729	
BND07	Transitional basalt	0.28291	0.000003	4.7	0.70383	0.000005	0.70378	39.111	15.623	18.840	
BND08	Transitional basalt	0.28282	0.000002	1.6	0.70509	0.000004	0.70499	38.689	15.554	18.333	
BND14	Transitional basalt	0.28290	0.000003	4.6	0.70381	0.000004	0.70376	39.071	15.618	18.802	
BND15	Alkaline basalt	0.28295	0.000003	6.2	0.70323	0.000003	0.70321	–	–	–	
BND18	Transitional basalt	0.28284	0.000003	2.4	0.70545	0.000004	0.70536	38.860	15.572	18.514	
BND20	Transitional basalt	0.28283	0.000004	2.0	0.70522	0.000004	0.70511	38.614	15.535	18.227	
BND02	Basaltic andesite	0.28278	0.000003	0.1	0.70448	0.000003	0.70439	38.519	15.575	17.979	
BND09	Basanite	0.28299	0.000003	7.6	0.70295	0.000004	0.70293	39.896	15.651	20.183	
BND10	Basanite	0.28298	0.000001	7.5	0.70295	0.000004	0.70293	39.917	15.655	20.193	
BND17	Hawaiite	0.28297	0.000002	6.9	0.70308	0.000003	0.70306	39.498	15.619	19.785	
BND19	Hawaiite	0.28297	0.000002	7.1	0.70311	0.000004	0.70311	39.517	15.621	19.841	
BND11	Trachyte	0.28258	0.000003	-6.6	0.71006	0.000003	0.70703	39.633	15.660	18.401	
BND12	Trachyte	0.28258	0.000003	-6.9	0.70927	0.000004	0.70601	39.620	15.662	18.400	
BND13	Trachyte	0.28258	0.000003	-6.8	0.70924	0.000004	0.70575	39.611	15.662	18.396	

CVL and reflect the heterogeneous nature of the mantle source. Alkaline lavas are close to the Mount Cameroon domain. Some mafic transitional lavas show low radiogenic Pb and high Sr ratios, suggesting that they interacted with the crust on their way to the surface.

## 7 Geochronology

Eight samples were subjected to K–Ar dating. The Ar isotopic data and calculated ages for the samples are presented in Table 3. The ages range from middle Eocene (47 Ma) to Pliocene (5 Ma). The volcanic events in the Bafoussam area took place in two periods: a mafic and felsic transitional volcanic episode between 47–35 Ma (divided into two episodes: a mafic and felsic transitional between 47–44 Ma and a transitional around 37–35 Ma) and an alkaline volcanic episode between 10 and 5 Ma. The mafic and felsic transitional episodes are in the interval of transitional volcanism of the Bamoun, Bangou, and Fotouni areas (K–Ar ages of 51–39 Ma; Fosso et al. 2005; Moundi et al. 2007; Okomo Atouba et al. 2016; Ngongang Tchikankou et al. 2020) and transitional episode to that of the eastern edge of the West Cameroon Highlands (K–Ar age of ~ 37 Ma; Lemdjou et al. 2020). The alkaline period corresponds to alkaline volcanic eruptions in the Bangou, and Bamenda mountains and the volcanic areas of Bafang, and the eastern edge of the West Cameroon

Highlands (K–Ar ages of 10–4 Ma; Fosso et al. 2005; Kamgang et al. 2013; Tchuimegnie Ngongang et al. 2015; Lemdjou et al. 2020).

## 8 Discussion: Origin and evolution of the magmas

### 8.1 Fractional crystallization and crustal contamination

The alkaline lavas show a very limited range of chemical evolution (Fig. 7). A strong decrease in MgO content associated with a low decrease in CaO and a constant or increasing Al<sub>2</sub>O<sub>3</sub> content with increasing Th indicates early fractionation of olivine and clinopyroxene.

Crystal fractionation tendencies are not clear in the transitional lavas, probably because they belong to different magmatic series of different ages. Decreasing MgO, CaO, and TiO<sub>2</sub> confirm the fractionation of clinopyroxene and oxides, as observed from the nature of phenocrysts in the lavas (Fig. 7). However, the near-constant Al<sub>2</sub>O<sub>3</sub> content shows that plagioclase is not a major mineral phase during differentiation and this observation is confirmed by the constant Sr content in these rocks (Fig. 8). Some samples appear to have lower Al<sub>2</sub>O<sub>3</sub> content, but it will be shown later on that these samples are those who suffered crustal contamination. The felsic transitional lavas are highly evolved, and their very low content in MgO, CaO,

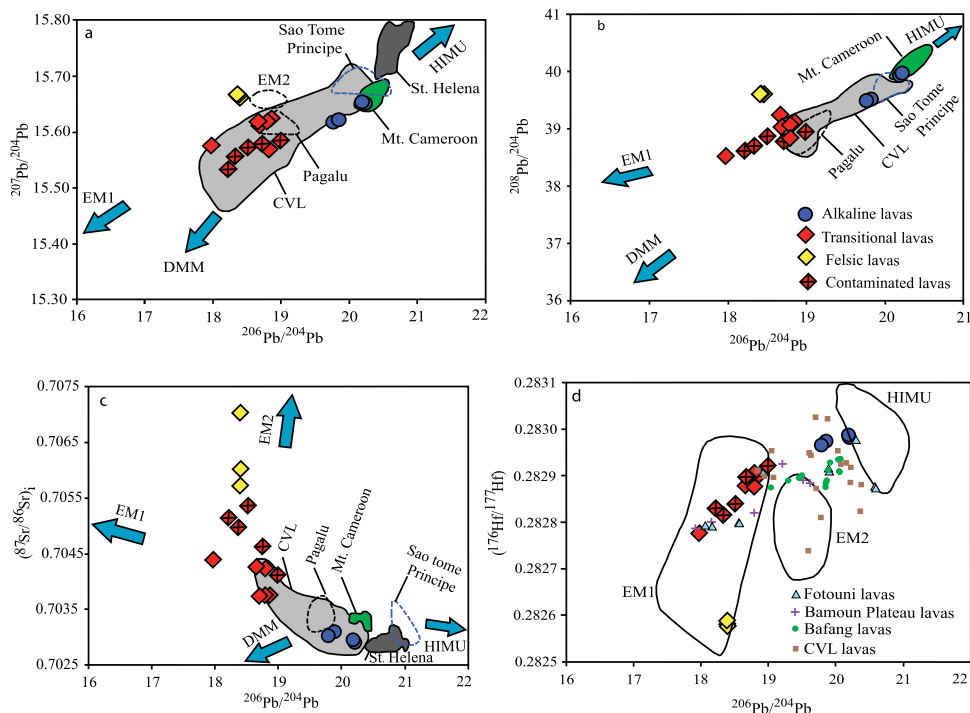


**Fig. 10** Isotopic compositions of the Bafoussam volcanic rocks: (a)  $^{207}\text{Pb}/^{204}\text{Pb}$  vs.  $^{206}\text{Pb}/^{204}\text{Pb}$ ; (b)  $^{208}\text{Pb}/^{204}\text{Pb}$  vs.  $^{206}\text{Pb}/^{204}\text{Pb}$ ; (c)  $(^{87}\text{Sr})/^{88}\text{Sr}$  vs.  $^{206}\text{Pb}/^{204}\text{Pb}$ ; (d)  $^{176}\text{Hf}/^{177}\text{Hf}$  vs.  $^{206}\text{Pb}/^{204}\text{Pb}$ . Principé, São Tomé and Pagalú data from Lee et al. (1994). The grey fields represent the data for the CVL and Mt. Cameroon (Halliday et al. 1988; Lee et al. 1994; Ballentine et al. 1997; Marzoli et al. 2000; Rankenburg et al. 2005; Yokoyama et al. 2007; Tsafack et al. 2009; Kamgang et al. 2013). St. Helena data from Chaffey et al. (1989), Hanyu et al. (2014), and Salters and White (1998). Data for Fotouni are from Ngongang Tchikankou et al. (2021), Bamoun Plateau from Okomo Atouba et al. (2016) and Bafang from Tchuimegnie Ngongang et al. (2015). Depleted MORB Mantle (DMM), Enriched Mantle 1 (EM1), Enriched Mantle 2 (EM2), High U/Pb Mantle (HIMU) from Hart (1984, 1988), Zindler and Hart (1986), Hart et al. (1992) and Hanan and Graham (1996). Legend as in Fig. 2. Red symbols with a cross represent the contaminated mafic lavas

**Table 3** K–Ar ages of Bafoussam lavas

Samples	Rocks	$\text{K}_2\text{O}$ (wt. %)	$^{40}\text{Ar}^* \cdot 10^{-7}\text{cm}^3/\text{g}$	$^{40}\text{Ar}^*/^{40}\text{Ar}_{\text{T}} (\%)$	$^{36}\text{Ar}$ exp. $10^{-9}\text{cm}^3$	Age (Ma)	Error ( $\pm 1$ sigma)
BND01	Transitional basalt	0.78	9.62	56.4	1.27	37.84	$\pm 0.94$
BND03	Transitional basalt	0.74	11.35	62.2	1.16	46.97	$\pm 1.14$
BND18	Transitional basalt	1.16	1.73	60.5	1.18	45.67	$\pm 1.12$
BND15	Alkaline basalt	1.33	4.24	47	0.81	9.85	$\pm 0.26$
BND02	Basaltic andesite	1.46	16.85	67.7	1.37	35.44	$\pm 0.85$
BND19	Hawaiite	1.59	2.32	32.4	0.83	4.52	$\pm 0.15$
BND13	Trachyte	5.29	75.74	92	1.11	43.87	$\pm 1.05$
BND12	Trachyte	5.2	76.27	95.8	0.58	44.93	$\pm 1.03$

and  $\text{TiO}_2$  is consistent with an evolution from the transitional mafic magmas through crystal fractionation. As for the mafic transitional rocks, their high  $\text{Al}_2\text{O}_3$  content is close to 14 wt.% indicates that plagioclase was not an important fractionating mineral during magma evolution in the transitional series.

Despite the low  $\text{SiO}_2$  content of most of the rocks, contamination by crustal rocks during magma evolution in

magma chambers cannot be excluded and must be evaluated before discussing the origin of the different magmas. AFC processes can be identified through the concomitant evolution of parameters evolving during crystal fractionation and parameters sensitive to contamination alone. Alkaline rocks have a constant  $\text{La}/\text{Nb}$  ratio close to 0.8 with evolving Th concentration and show no sign of contamination (Fig. 11a). The transitional samples show contrasting behaviour. Some

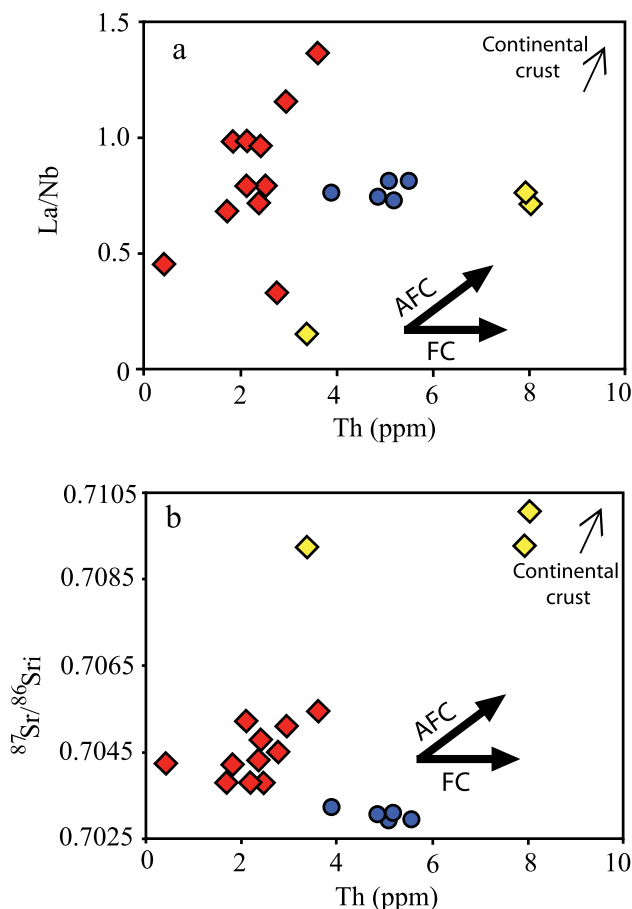


**Fig. 11** **a** La/Nb vs. Th diagram for alkaline, transitional and felsic lavas from Bafoussam. **b**  $^{87}\text{Sr}/^{86}\text{Sr}$  vs. Th diagram for the Bafoussam Lavas. Assimilation-Fractional Crystallization (AFC) and Fractional Crystallization (FC) vectors are drawn for the illustration of the element behavior during these processes

samples have also La/Nb ratio close to 0.8, while five samples form a positive correlation between La/Nb and Th. These magmas have probably interacted with a crustal component with higher Th content, and a high La/Nb ratio, as expected from crustal rocks. These samples also have the lowest  $\text{Al}_2\text{O}_3$  content of the transitional rocks (Fig. 7). This observation is one of the rare cases where crustal contamination can be seen on major elements and indicates that the contaminant must be a low-Al crustal rock. One felsic and two mafic samples have a very low La/Nb ratio but are also among the most altered rocks (LOI ranging from 1.7 to 3 wt.%). In the Sr isotopes – Th diagram (Fig. 11b), the alkaline lavas have a very low  $^{87}\text{Sr}/^{86}\text{Sr}$  ratio, with no correlation with Th. On the opposite, a strong correlation is drawn by some of the transitional samples, with increasing Sr isotopic ratio along differentiation. The samples involved in this correlation are mostly those with a high La/Nb ratio. This correlation confirms that some transitional samples interacted with rocks from the crust. Interestingly, the felsic

samples have La/Nb ratio similar to the non-contaminated mafic samples but belong to the contamination trend regarding their Sr isotopic ratio. They were probably contaminated by crustal rocks with a low La/Nb ratio. The pattern of contamination for the felsic rocks is different from what can be seen on the mafic ones. While contamination of the mafic magmas drags their Pb isotopic compositions towards lower ratios, the trachytes have higher  $^{207}\text{Pb}/^{204}\text{Pb}$  and  $^{208}\text{Pb}/^{204}\text{Pb}$  than the mafic rocks, for similar  $^{206}\text{Pb}/^{204}\text{Pb}$  (Fig. 10). They also have  $\text{Al}_2\text{O}_3$  content higher than the mafic contaminated rocks. Contamination of the transitional magmas appears to have occurred in two different steps, and probably in two different places. Mafic samples did not fractionate plagioclase and were contaminated in deep magma chambers by low  $\text{Al}_2\text{O}_3$  crustal rocks. Trachytes show some evidence for plagioclase fractionation (low Sr and negative Eu anomaly) and were contaminated by high  $^{207}\text{Pb}/^{204}\text{Pb}$  and  $^{208}\text{Pb}/^{204}\text{Pb}$  and low La/Nb crustal rocks, probably in shallower magma chambers.

In conclusion, along with the felsic rocks, transitional samples BND1, BND6, BND8, BND18, and BND20 have interacted with crustal rocks and their chemical and isotopic compositions have been changed enough that they cannot be used to study the mantle source of the Bafoussam volcanic rocks.

## 8.2 Mantle source

The origin and the source of the magmatism along the Cameroon Volcanic Line (CVL) is a subject of discussion within the scientific community. Several models taking into consideration geochemical and geophysical data have been proposed, including melting of the St Helena mantle plume head (Halliday et al. 1988; Lee et al. 1994; Ballentine et al. 1997; Rankenburg et al. 2005), weak upper mantle convective melting (Fitton and Dunlop 1985), or mantle melting due to edge-driven convection along the Congo craton or due to linear mantle instabilities beneath the continent (Reusch et al. 2010, 2011; Milelli et al. 2012; Fourel et al. 2013). Several studies have been conducted on mantle xenoliths along the CVL and have shown that the mantle beneath the CVL is made of peridotite and pyroxenite. The diversity of their mineralogical and chemical composition (peridotite and pyroxenite) shows that the mantle beneath the CVL is highly heterogeneous (Lee et al. 1996; Temdjam et al. 2004; Teitchou et al. 2011; Nguihdama et al. 2014; Njombie Wagsong et al. 2021; Tedonkenfack et al. 2021). The chemical and isotopic composition of the magmatism presents all along the CVL allows us to discuss the composition of the mantle source of the magmas, but also the depth of melting, the mineralogy of the melting mantle, and the evolution of the mantle source during time. The data obtained on the

Bafoussam lavas extend some observations already done in other volcanic provinces of the CVL and bring some more constraints on the origin of the magmas along the CVL.

Rare earth elements in alkaline and transitional mafic lavas from Bafoussam show patterns (Fig. 9) enriched in light REE (LREE) and with low content of heavy REE (HREE). These rocks are different from normal MORB and come from a mantle source enriched in incompatible elements compared to the asthenospheric mantle. The low HREE abundances can be explained by the presence of residual garnet in the mantle source. HREE are highly compatible in garnet and thus retained in the residual mantle during melting. The Th/Yb ratio in magmas is very sensitive to the presence of garnet in the source (Wang et al. 2002). Both alkaline and transitional lavas from Bafoussam have elevated  $(\text{Th}/\text{Yb})_n$  ratios (Fig. 12a), indicating an origin from a garnet-bearing mantle source, at a depth of more than 80 km. Accordingly, the differences

in the two magmatic series cannot be attributed to the mineralogy of their source.

Incompatible trace elements are very sensitive to the source mineralogy and to the extent of melting. Ce/Y and Zr/Nb can be used to evaluate the amount of garnet in the source, as well as the degree of melting at the origin of the studied rocks (Hardarson and Fitton 1991). The diagram of Fig. 12b confirms the presence of garnet in the source for both series and indicates higher melting degrees for the transitional lavas (between 3 and 5%) than for the alkaline lavas (lower than 2.5%). These lower melting degrees for the alkaline lavas can explain their higher incompatible element contents, especially in Th, Nb, Zr, and LREE (Figs. 8, 9). This is confirmed in the Ni vs. Th diagram (Fig. 13) in which the two series are different. The low Ni content for the transitional rocks confirms they are far from the composition of primary magmas, and that they underwent strong olivine fractionation. The large dispersion of the data is probably related to the presence of several magmatic series with different primary magmas. Ni content is higher in the alkaline rocks, but still lower than what is expected in primary mantle melts. The strong decrease of the Ni content with increasing Th is also consistent with olivine fractionation. Despite this similar evolution, extrapolation of the Th content towards high Ni content confirms that the primary melts at the origin of the two series are quite different, with higher Th content in the magmas at the origin of the alkaline series. This difference in the trace element composition of the primary melts for the two series can be caused by different melting degrees of a single source, or by partial melting of two different mantle sources with different trace element compositions.

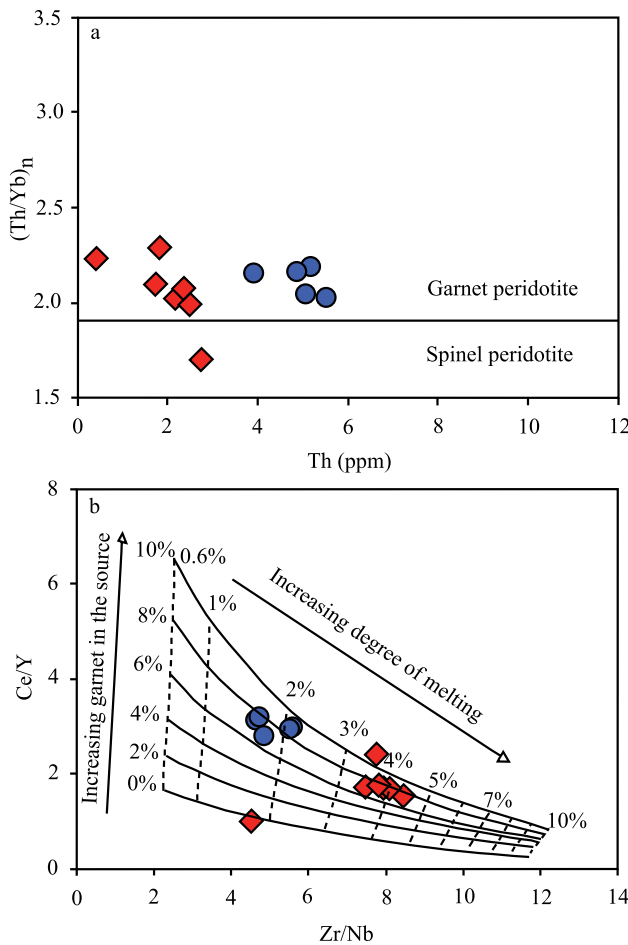


**Fig. 12** Trace element variations and origin of the mafic lavas: **a** ( $\text{Th}/\text{Yb}$ )<sub>n</sub> vs. Th diagram showing the melt domains of garnet and spinel peridotite (Wang et al. 2002); **b** Ce/Y vs. Zr/Nb showing residual garnet contents and melting degrees in the mantle (Hardarson and Fitton 1991). Legend as in Fig. 2

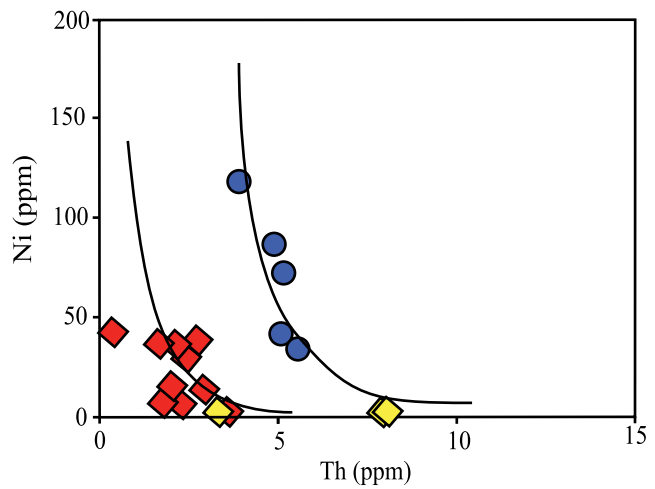


**Fig. 13** Ni vs. Th diagram. Two groups of samples are visible, one made of transitional and felsic lavas, while the other one contains alkaline lavas. The two black lines represent very simple models of olivine fractionation starting from a primary magma with 300 ppm Ni and 1 ppm or 4 ppm Th. Legend as in Fig. 2

The isotopic composition of the uncontaminated rocks from the two series shows that they originate from different mantle sources. The alkaline rocks have isotopic compositions more akin to the HIMU component. They always plot close to the recent lavas from Mount Cameroon (Yokoyama et al. 2007) and also from recent alkaline lavas from volcanic massifs nearby (Tchuimegnie Ngongang et al. 2015; Okomo Atouba et al. 2016; Ziem à Bidias et al. 2018; Ngongang Tchikankou et al. 2020). On the opposite, the transitional lavas have different isotopic compositions, with lower Pb and Hf and higher Sr isotopic ratios (Fig. 10). In the Pb-Pb isotopic plots (Fig. 10a, b) the Bafoussam lavas define a mixing line between two different components. One component is well identified in the recent volcanism of the CVL and has similar Pb isotopic composition to the lavas from Mount Cameroon. The second mantle component has very low Pb isotopic ratios and is also present in all the oldest lavas from the CVL. Combining Pb isotopes with Sr and Hf isotopic compositions allows us to put some more constraints on the nature and composition of these mantle sources. While the high Pb isotopes mantle source present in the alkaline lavas is close to the source of the Mount Cameroon lavas in the Pb-Pb plots (Fig. 10a, b), it has higher Hf and lower Sr isotopic ratios (Fig. 10c, d) and represents a different mantle source. Mount Cameroon, close to the continent-ocean boundary is tapping a unique mantle source, different from the alkaline lavas located further inland along the CVL.

The low Pb isotopes mantle source of the Bafoussam transitional lavas seems to be similar to the oldest rocks of the CVL in the different volcanic massifs. It has low Hf and high Sr isotopic composition and these lavas plot towards the EMI mantle component. It is noticeable that none of the Bafoussam transitional lavas plot into the direction of the DMM component, characteristics of the depleted asthenospheric mantle, in agreement with the source of the CVL lavas being located in the subcontinental lithospheric mantle. Many transitional lavas from Bafoussam display a positive Eu anomaly (Fig. 9b). They do not contain any cumulative plagioclase and their high alumina content show that plagioclase was not a major fractionating phase during their evolution in the crust. This chemical characteristic is thus inherited from their mantle source. It has already been observed in other volcanic massifs from the CVL (Marzoli et al. 2000; Kamgang et al. 2013; Tchuimegnie Ngongang et al. 2015) and is consistent with the melting of pyroxenites disseminated in the lithospheric mantle. It appears that the source of the transitional lavas is probably a mixture of peridotite and pyroxenite, as pyroxenites from Cameroon as well as from other localities have been shown to have high Eu content due to ancient plagioclase abundances in their protolith (France et al. 2015). This part of the lithospheric mantle beneath

Cameroon was probably refertilized by melt circulation during which pyroxenites formed, maybe during Pan-African orogenic events, before being melted again from the beginning of the CVL formation.

It appears that met formation beneath the CVL is governed by the melting of two different mantle sources, present all along the CVL. One is a pyroxenite-bearing mantle and produced magmas during the first and main part of the CVL formation. These magmas are formed by moderate degrees of melting and are of transitional affinity. With time, the magma composition changes. The melting of pyroxenite stops and the magmas are generated through lower melting degrees, thus becoming more and more alkaline, and from a mantle source with different trace and isotopic composition, especially with higher Pb isotopic ratios. Asthenospheric mantle sources are not participating in the melt generation and the two different mantle sources seem to be located in the lithospheric mantle. The heterogeneity of this lithospheric mantle is even more complicated, as the source at the origin of the magmas emitted by Mount Cameroon is different from the source of the alkaline magmas along the CVL, as confirmed by other studies (Okomo Atouba et al. 2016; Ziem à Bidias et al. 2018; Ngongang Tchikankou et al. 2020). The location of the source of magmas along the CVL in the lithospheric mantle is consistent with the most recent models concerning the CVL origin, demonstrating the possible development of lithospheric instabilities along the edge of continents. Such instabilities develop over long timescales due to large lateral variations in lithospheric thickness (Milelli et al. 2012; Fourel et al. 2013; De Plaen et al. 2014).

## 9 Conclusion

Volcanism in the Bafoussam area, in the central part of the Cameroon Volcanic Line, spans a large range of ages, from 47 to less than 5 Ma. The oldest volcanism is of transitional affinity, with mafic and felsic rocks, while since 10 Ma volcanism is alkaline and only mafic. Magmas evolved in the crust through fractionation of olivine and clinopyroxene, while plagioclase was not a major crystallizing phase. Some transitional magmas were contaminated during interactions with crustal rocks. Uncontaminated rocks from both series are enriched in incompatible elements. Their formation involved two different mantle sources, an enriched mantle with low Pb isotopic composition and containing some amounts of pyroxenites for the transitional magmas, and an enriched mantle without pyroxenite but with high Pb isotopic ratios for the alkaline melts. These two mantle sources are probably located in the lithospheric mantle, and the asthenosphere is not involved in the source of the two series. These observations

are consistent with the absence of any mantle plume beneath the CVL, but rather partial melting of the lithospheric mantle in response to edge convection along the margin of the Congo craton.

**Supplementary Information** The online version contains supplementary material available at <https://doi.org/10.1007/s11631-022-00560-z>.

**Acknowledgements** Céline Liorzou and Jessica Langlade are thanked for their help in the acquisition of chemical results. Thanks also to an anonymous reviewer who provided constructive advice.

## Declarations

**Conflict of interest** The authors declare that they have no conflict of interest.

## References

- Adams AN, Wiens DA, Nyblade AA, Euler GG, Shore PJ, Tibi R (2015) Lithospheric instability and the source of the Cameroon Volcanic Line: evidence from Rayleigh wave phase velocity tomography. *J Geophys Res* 120:1708–1727
- Ballentine CJ, Lee D-C, Halliday AN (1997) Hafnium isotopic studies of the Cameroon line and new HIMU paradoxes. *Chem Geol* 139:111–124
- Bardintzeff J-M, Nkouandou OF, Mefire AF (2020) First occurrence of pigeonite in the Cameroon Volcanic Line. *Arab J Geosci* 13:3–14
- Bellon H, Quoc Buü N, Chaumont J, Philippot JC (1981) Implantation ionique d'argon dans une cible support: application au traçage isotopique de l'argon contenu dans les minéraux et les roches. *Comptes Rendus De L'académie Des Sciences, Paris* 292:977–980
- Binns RA, Duggan MB, Wilkerson JF (1970) High pressure megacrysts in alkaline lavas from north-eastern New South Wales. *Am J Sci* 269:132–168
- Buddington AF, Lindsley DH (1964) Iron-titanium oxide minerals and synthetic equivalents. *J Petrol* 5:310–357
- Burke K (2001) Origin of the Cameroon line of volcano-capped swells. *J Geol* 109:349–362
- Chaffey DJ, Cliff RA, Wilson BM (1989) Characterization of the St. Helena magma source magmatism in the Ocean Basins. In: Saunders AD, Norry MJ.(Eds.), Geological Society of London, London, 257–276
- Cotten J, Le Dez A, Bau M, Caroff M, Maury RC, Dulski P, Fourcade S, Bohn M, Brousse R (1995) Origin of anomalous rare-earth element and yttrium enrichments in subaerially exposed basalts: evidence from French Polynesia. *Chem Geol* 119:115–138
- De Plaen RSM, Bastow ID, Chambers EL, Keir D, Gallacher RJ, Keane J (2014) The development of magmatism along the Cameroon Volcanic Line: Evidence from seismicity and seismic anisotropy. *Journal of Geophysical Research: Solid Earth* 119:4233–4252
- Déruelle B, Ngounouno I, Demaiffe D (2007) The Cameroon hot line (CHL): A unique example of active alkaline intraplate structure in both oceanic and continental lithospheres. *CR Geosci* 339:589–600
- Djouka-Fonkwe ML, Schulz B, Schüssler U, Tchouankoué J-P, Nzolang C (2008) Geochemistry of the Bafoussam Pan-African I- and S-type granitoids in western Cameroon. *J Afr Earth Sc* 50:148–167
- Dumort JC (1968) Notice explicative sur la feuille Douala-Ouest + Cartes géologiques de la reconnaissance à l'échelle de 1/50000. République Fédérale du Cameroun, Bureau de Recherches Géologiques et Minières, Cameroun, pp 68
- Farahat ES, Abdel Ghani MS, Aboazom AS, Asran AMH (2006) Mineral chemistry of Al Haruj low-volcanicity rift basalts, Libya: Implications for petrogenetic and geotectonic evolution. *J Afr Earth Sc* 45:198–212
- Fitton JG, Dunlop HM (1985) The Cameroon Line, west Africa, and its bearing on the origin of oceanic and continental alkali basalt. *Earth Planet Sci Lett* 72:23–38
- Fitton JG (1987) The Cameroon Line: West Africa: A comparison between oceanic and continental alkaline volcanism, In Fitton JG, and Upton, BGJ, eds., *Alkaline Igneous Rocks*. Geological Society of London Special Publication 30, 273–291.
- Fosso J, Ménard JJ, Bardintzeff JM, Wandji P, Tchoua FM, Bellon H (2005) Les laves du Mont Bangou: Une première manifestation volcanique éocène, à affinité transitionnelle de la ligne du Cameroun. *CR Geosci* 337:315–325
- Fourel L, Milelli L, Jaupart C, Limare A (2013) Generation of continental rifts, basins, and swells by lithosphere instabilities. *Journal of Geophysical Research: Solid Earth* 118:3080–3100
- France L, Chazot G, Kornprobst J, Dallai L, Vannucci R, Grégoire M, Bertrand H, Boivin P (2015) Mantle refertilization and magmatism in old orogenic regions: The role of late orogenic pyroxenites. *Lithos* 232:49–75
- Gountié Dedzo M, Asaah ANE, Fozing ME, Tchamabé CB, Zangmo TG, Nguihdama D, Seuwui DT, Kamgang P, Aka FT, Ohba T (2019) Petrology and geochemistry of lavas from Gawar, Minawao and Zamay volcanoes of the northern segment of the Cameroon volcanic line (Central Africa): Constraints on mantle source and geochemical evolution. *J Afr Earth Sc* 153:31–41
- Green DH (1976) Experimental studies on a modal upper mantle composition at high pressure under water saturated and water undersaturated conditions. *Can Mineral* 14:255–268
- Halliday AN, Dickin AP, Fallick AE, Fitton FG (1988) Mantle dynamics: A Nd, Sr, Pb and O isotopic study of the Cameroon line volcanic chain. *J Petrol* 45:318–332
- Halliday AN, Davidson JP, Holden P, Dewolf C, Lee D-C, Fitton JG (1990) Trace-element fractionation in plumes and the origin of HIMU mantle beneath the Cameroon line. *Nature* 347:523–528
- Hanan BB, Graham DW (1996) Lead and helium isotope evidence from oceanic basalts for a common deep source of mantle plumes. *Science* 272:991–995
- Hanyu T, Kawabata H, Tatsumi Y, Kimura J-I, Hyodo H, Sato K, Miyazaki T, Chang Q, Hirahara Y, Takahashi T, Senda R, Nakai S (2014) Isotope evolution in the HIMU reservoir beneath St. Helena: Implications for the mantle recycling of U and Th. *Geochim Cosmochim Acta* 143:232–252
- Hardarson BS, Fitton JG (1991) Increased mantle melting beneath Snaefellsjökull volcano during Late Pliocene deglaciation. *Nature* 353:62–64
- Hart SR (1984) The Dupal anomaly: a large-scale isotopic anomaly in the southern hemisphere. *Nature* 309:753–756
- Hart SR (1988) Heterogeneous mantle domains: Signatures, genesis and mixing chronologies. *Earth Planetary Sci Letters* 90:273–296
- Hart SR, Hauri EH, Oschmann LA, Whitehead JA (1992) Mantle plumes and entrainment: isotopic evidence. *Science* 256:517–520
- Hirschmann M, Ghirosso MS (1994) Activities of Ni-, Co-, and Mn-silicate in magmatic liquids and applications to olivine/liquid and to silicate/metal partitioning. *Geochim Cosmochim Acta* 58:4109–4126
- Irvine TN, Barragar WRA (1971) A guide to chemical classification of the common volcanic rocks. *Can J Earth Sci* 8:523–548

- Kamgang P, Njonfang E, Nono A, Gountié Dedzo M, Tchoua FM (2010) Petrogenesis of a silicic magma system: geochemical evidence from Bamenda Mountains, NW Cameroon, Cameroon Volcanic Line. *J Afr Earth Sc* 58:285–304
- Kamgang P, Chazot G, Njonfang E, Tchuimegnie Ngongang NB, Tchoua MF (2013) Mantle sources and magma evolution beneath the Cameroon Volcanic Line: Geochemistry of mafic rocks from the Bamenda Mountains (NW Cameroon). *Gondwana Res* 24:727–741
- Kimura J-I, Ariskin AA (2014) Calculation of water-bearing primary basalt and estimation of source mantle conditions beneath arcs: PRIMACALC2 model for WINDOWS Geochemistry. *Geophysics, Geosystems* 15:1494–1514
- King SD, Ritsema J (2000) African hot spot volcanism: small-scale convection in the upper mantle beneath cratons. *Science* 290:1137–1140
- Köhler T, Brey GP (1990) Ca-exchange between olivine and clinopyroxene as a geothermobarometer calibrated from 2 to 60 kbar in primitive natural Iherzolites. *Geochim Cosmochim Acta* 54:2375–2388
- Kuepouo G, Tchouankoué JP, Nagao T, Sato H (2006) Transitional tholeiitic basalts in the tertiary Bana volcano-plutonic complex, Cameroon Line. *J Afr Earth Sc* 45:318–332
- Le Bas MJ, Le Maitre RW, Streckeisen B (1986) A chemical classification of volcanic rocks based on the total alkali-silicic diagram. *J Petrol* 27:745–750
- Lee DC, Halliday AN, Fitton GJ, Poli G (1994) Isotopic variations with distance and time in the volcanic islands of the Cameroon Line: evidence of the mantle plume origin. *Earth Planet Sci Lett* 123:119–138
- Lee D-C, Halliday AN, Davies GR, Essene EJ, Fitton G, Temdjm R (1996) Melt enrichment of shallow depleted mantle: a detailed petrological, trace element and isotopic study of mantle-derived xenoliths and megacrysts from Cameroun line. *J Petrol* 37:415–437
- Lemdjou YB, Zhang D, Tchouankoué JP, Hu J, Tchuimegnie Ngongang NB, Soh Tamehe L, Yuan Y (2020) Elemental and Sr-Nd-Pb isotopic compositions, and K-Ar ages of transitional and alkaline plateau basalts from the eastern edge of the West Cameroon Highlands (Cameroon Volcanic Line). *Lithos* 105414:358–359
- Marzoli A, Renne PR, Piccirillo EM, Castorina F, Bellieni G, Melfi AJ, Nyobe JB, N'ni, J. (1999) Silicic magmas from the continental Cameroon Volcanic Line (Oku, Bambouto and Ngaoundere):  $^{40}\text{Ar}$ - $^{39}\text{Ar}$  dates, petrology, Sr-Nd-O isotopes and their petrogenetic significance. *Contrib Miner Petrol* 135:133–150
- Marzoli A, Renne PR, Piccirillo EM, Francesca C, Bellieni G, Melfi AJ, Nyobe JB, N'ni, J. (2000) The Cameroon Volcanic Line Revisited: petrogenesis of continental basaltic magmas from lithospheric and asthenospheric mantle sources. *J Petrol* 41:87–109
- McDonough, WF (2003) Compositional models for Earth's core. In the mantle and core (ed.R.W. Carlson) vol.2. Treatise on Geochemistry (eds. H.D. Holland and K.K. Turekian). Elsevier-pergamon, Oxford, 547–568.
- Merle R, Marzoli A, Aka FT, Chiariadis JM, Reisberg L, Castorina F, Jourdan F, Renne PR, N'ni, J., Nyobe, J.B. (2017) Mt Bambouto Volcano, Cameroon Line: Mantle Source and Differentiation of Within-plate Alkaline Rocks. *J Petrol* 58:933–962
- Middlemost EAK (1975) The Basalt Clan Earth Sciences Review 11:337–364
- Milelli L, Fourel L, Jaupart C (2012) A lithospheric instability origin for the Cameroon Volcanic Line. *Earth Planet Sci Lett* 335–336:80–87
- Morimoto N, Fabries J, Ferguson AK, Ginzburg IV, Ross M, Seifert FA, Zussmann J, Aoki K, Gottardi G (1988) Nomenclature of pyroxenes. *Am Miner* 173:1123–1133
- Moundi A, Wandji P, Bardintzeff JM, Menard J-J, Okomo Atouba LC, Mouncherou O. F, Reusser E, Bellon H, Tchoua, F M (2007) Les basaltes éocènes à affinité transitionnelle du plateau Bamoun, témoin d'un réservoir mantellique enrichi sous la ligne du Cameroun. *Comptes Rendus Géoscience* 339, 396–406.
- Ngako V, Njonfang E, Aka Tongwa F, Affaton P, Nnange Metuk J (2006) The north south Paleozoic to Quaternary trend of alkaline magmatism from Niger-Nigeria to Cameroon: Complex interaction between hotspots and Precambrian faults. *J Afr Earth Sc* 45:241–256
- Ngongang Tchikankou NL, Kamgang P, Chazot G, Agranier A, Bellon H, Nonnotte P, Tchuimegnie Ngongang NB, Kwekam M (2020) Mantle source evolution beneath the Cameroon volcanic line: geochemical and geochronological evidences from Fotouni volcanic series, Western Cameroon. *Arab J Geosci* 13:2–20
- Ngonge ED, Hollanda MHBM, Nkongui Nsifa E, Tchoua FM (2014) Petrology of the Guenfalabo ring-complex: An example of a complete series along the Cameroon Volcanic Line (CVL), Cameroon. *J Afr Earth Sc* 96:139–154
- Ngounounou I, Moreau C, Déruelle B, Demaiffe D, Montigny R (2001) Pétrologie du complexe alcalin sous-saturé de Kokoumi (Cameroun). *Bulletin De La Société Géologique De France* 172:675–686
- Ngounounou I, Déruelle D, Demaiffe D, Montigny R (2003) Petrology of the bimodal Cenozoic volcanism of the Upper Benue valley, northern Cameroon (Central Africa). *Contrib Miner Petrol* 145:87–106
- Nguihdam D, Chazot G, Kamgang P, Mbowou Gbambié IB, Ngounounou I (2014) Spinel-Bearing Lherzolite Xenoliths from Hosséré Garba (Likok, Adamawa-Cameroun): Mineral Compositions and Geothermobarometric Implications. *Int J Geosci* 5:1435–1444
- Njombie Wagsong MP, Temdjm R, Tchuimegnie Ngongang BN, Foley FS, Mebara Onana XF (2021) Pyroxenite in the mantle source of basanites at the Youkou maar, Adamawa Volcanic Massif (Cameroon Volcanic Line, West Africa). *Chem Geol* 583:120478
- Njome SM, De Wit JM (2014) The Cameroon Line: Analysis of an intraplate magmatic province transecting both oceanic and continental lithospheres. Constraints, controversies and models. *Earth Sci Rev* 139:168–194
- Okomo Atouba CL, Chazot G, Moundi A, Agranier A, Bellon H, Nonnotte P, Nzenti JP, Kankeu B (2016) Mantle beneath the Cameroon Volcanic Line: geochemistry and geochronology of the Bamoun plateau mafic rocks. *Arabian Journal of Geoscience* 9(4):270
- Pouclet A, Kagou Dongmo A, Bardintzeff JM, Wandji P, Tagheu PC, Nkouathio D, Bellon H, Ruffet G (2014) The Mount Manengouba, a complex volcano of the Cameroon line: volcanic history, petrological and geochemical features. *J Afr Earth Sc* 97:297–321
- Rankenburg K, Lassister JC, Brey G (2005) The role of continental crust and lithospheric mantle in the genesis of Cameroon volcanic line lavas: Constraints from isotopic variations in lavas and megacrysts from the Bui and Jos Plateaux. *J Petrol* 46:169–190
- Reusch AM, Nyblade AA, Wiens DA, Shore, P.J., Ateba, B., Tabod, C.T., Nnange, J.M. (2010) Upper mantle structure beneath Cameroon from body wave tomography and the origin of the Cameroon Volcanic Line. *Geochem Geophys Geosyst* 11:1–17
- Reusch AM, Nyblade AA, Tibi R, Wiens DA, Shore PJ, Bekoa A, Tabod CT, Nnange JM (2011) Mantle transition zone thickness

- beneath Cameroon: evidence for an upper mantle origin for the Cameroon Volcanic Line. *Geophys J Int* 187:1146–1150
- Salter VJM, White WM (1998) Hf isotope constraints on mantle evolution. *Chem Geol* 145:447–460
- Simkin T, Smith JV (1970) Minor-element distribution in olivine. *J Geol* 78:304–325
- Smith JV, Brown WL (1988) Feldspar Minerals, Second Revised and Extended. Springer Verlag, Berlin, Heidelberg, New York, London, Paris, Tokyo
- Suh CE, Sparks RSJ, Fitton JG, Ayonghe SN, Annen C, Nana R, Luckmen A (2003) The 1999 and 2000 eruptions of Mount Cameroon: Eruption behaviour and petrochemistry of lava. *Bull Volcanol* 65:267–281
- Sun S, McDonough W (1989) Chemical and isotopic systematics of ocean basalts: implications for mantle composition and processes. *Geological Society of London Special Publication* 42:313–345
- Tchoua, F. M. 1974. Contribution à l'étude géologique et pétrographique de quelques volcans de la Ligne du Cameroun (Monts Manengouba et Bambouto). Thèse d'Etat, Université de Clermont-Ferrand U.E.R. Sciences exactes et naturelles, 337p.
- Tchuimegnie Ngongang NB, Kamgang P, Chazot G, Agranié A, Bellon H, Nonnotte P (2015) Age, geochemical characteristics and petrogenesis of Cenozoic intraplate alkaline volcanic rocks in the Bafang region, West Cameroon. *J Afr Earth Sc* 102:218–232
- Tedonkenfack SST, Puziewicz J, Aulbach S, Ntaflos T, Kaczmarek MA, Matusiak-Małek M, Kukuła A, Ziobro M (2021) Lithospheric mantle refertilization by DMM-derived melts beneath the Cameroon Volcanic Line—a case study of the Befang xenolith suite (Oku Volcanic Group, Cameroon). *Contrib Miner Petrol* 176:37
- Teitchou MI, Grégoire M, Temdjim R, Ghogomu RT, Ngwa C, Aka FT (2011) Mineralogical and geochemical fingerprints of mantle metasomatism beneath Nyos volcano (Cameroon volcanic line). *The Geological Society of America Special Paper* 478:193–210
- Temdjim R, Boivin P, Chazot G, Robin C, Rouleau E (2004) L'hétérogénéité du manteau supérieur à l'aplomb du volcan de Nyos (Cameroun) révélée par les enclaves ultrabasiques. *CR Geosci* 336:1239–1244
- Tsafack J, - P. F., Wandji, P., Bardintzeff, J. - M., Bellon, H., Guillou, H. (2009) The Mount Cameroon stratovolcano (Cameroon Volcanic Line, Central Africa): petrology, geochemistry, isotope and age data. *Mineral Petrol* 47:65–78
- Wang K, Plank T, Walker JD, Smith EI (2002) A mantle melting profile across the Basin and Range, SW USA. *J Geophys Res* 107:1–21
- Yokoyama T, Aka FT, Kusakabe M, Nakamura E (2007) Plume-lithosphere interaction beneath Mt. Cameroon volcano, West Africa: constraints from  $^{238}\text{U}$ - $^{230}\text{Th}$ - $^{226}\text{Ra}$  and Sr-Nd-Pb isotopes systematics. *Geochim Cosmochim Acta* 71:1835–1854
- Ziem à Bidias, L. A., Chazot, G., Moundi, A., Nonnotte, P. (2018) Extreme source heterogeneity and complex contamination patterns along the Cameroon Volcanic Line: New geochemical data from the Bamoun plateau. *CR Geosci* 350:100–109
- Zindler A, Hart SR (1986) Chemical geodynamics. *Annual Reviews of Earth and Planetary Science* 14:493–571

Springer Nature or its licensor holds exclusive rights to this article under a publishing agreement with the author(s) or other rightsholder(s); author self-archiving of the accepted manuscript version of this article is solely governed by the terms of such publishing agreement and applicable law.